5-2023

Enabling Premixed Hydrogen-Air Combustion for Aeroengines via Laboratory Experiment Modeling

Christopher James Caulfield
University of Tennessee Space Institute, ccaulfi3@vols.utk.edu

To the Graduate Council:

I am submitting herewith a thesis written by Christopher James Caulfield entitled "Enabling Premixed Hydrogen-Air Combustion for Aeroengines via Laboratory Experiment Modeling." I have examined the final electronic copy of this thesis for form and content and recommend that it be accepted in partial fulfillment of the requirements for the degree of Master of Science, with a major in Aerospace Engineering.

Paul P. Palies, Major Professor

We have read this thesis and recommend its acceptance:

Paul P. Palies, Trevor Moeller, Mark Gragston

Accepted for the Council:
Dixie L. Thompson

Vice Provost and Dean of the Graduate School

(Original signatures are on file with official student records.)

Enabling Premixed Hydrogen-Air Combustion for Aeroengines via Laboratory Experiment Modeling

A Thesis Presented for the

Master of Science

Degree

The University of Tennessee, Knoxville

Christopher James Caulfield

May 2023

This thesis presented by Christopher Caulfield is dedicated to Dr. Steven R. Anton of the mechanical engineering department at Tennessee Technological University. He believed in me when I did not believe in myself.

Acknowledgments

I would like to thank everyone who helped me get to this point. From my friends, to fellow researchers, and mentors. I would like to take this time and thank Dr. Palies, Dr. Gragston, and Dr. Moeller for helping and serving on my committee. This work would not have been possible without the instruction and guidance of Dr. Palies. Without the support and guidance of my friends and mentors this research would have not occurred. I am grateful to the turbomachinery and propulsion team at Ansys for their collaboration and teaching during the internship. I am truly thankful for everyone's assistance and advice.

Abstract

All combustion systems from large scale power plants to the engines of cars to gas turbines in aircraft are looking for new fuel sources. Recently, clean energy for aviation has come into the foreground as an important issue due to the environment impacts of current combustion methods and fuels used. The aircraft industry is looking towards hydrogen as a new, powerful, and clean fuel of the future. However there are several engineering and scientific challenges to overcome before hydrogen can be deployed into the industry. These issues range from storing the hydrogen in a viable cryogenic form for an aircraft to stably burning the hydrogen in different phases during flight. Since a fundamental aspect, the fuel source (usually kerosene), is being switched to hydrogen, extensive modeling and ground testing of a future engine is required before a gas turbine engine can be retrofitted to work with hydrogen or built from the ground up. Modeling and simulating turbofan engine components can complement the engineering design process by allowing designs to be tested before being implemented into an actual turbofan engine. This allows an engineer to build confidence around a given design. Actual testing of gas turbine engines and their turbomachinery components is expensive and modeling these devices can help mitigate some of the cost and address problems early on in the design of the engine. In this thesis, several models are developed that allow for the study of hydrogen in a laboratory environment, and are compared to past literature, industrial software and computational models. This includes a 0D turbofan engine model and computational fluid dynamics simulations of a laboratory scale burner. The results formed in this work establish that the initial design of the burner and codes developed here can serve as a foundation for future experiments and aid in the pursuit of achieving a gas turbine engine operating with hydrogen-air mixtures.

Table of Contents

List of Tables

List of Figures

Nomenclature

a	=	Speed of sound [m s^{-1}]
AFR	=	Air to Fuel ratio
c	=	Reaction progress variable
c_p	=	Specific heat capacity at constant pressure [J [kg K]$^{-1}$]
$c_{p,c}$	=	Specific heat capacity of cold air [J [kg K]$^{-1}$]
$c_{p,h}$	=	Specific heat capacity of hot air [J [kg K]$^{-1}$]
D	=	Diameter [m]
Da	=	Damköhler number
hpr	=	Fuel heating value [J kg^{-1}]
FAR	=	Fuel to Air ratio
Ka	=	Karlovitz number
l_t	=	Turbulence Integral length scale [m]]
Ma	=	Mach number
$\dot{m}_b$	=	Fan bypass mass flowrate [kg s^{-1}]
$\dot{m}_c$	=	Engine core mass flowrate [kg s^{-1}]
$\dot{m}_f$	=	Fuel mass flowrate [kg s^{-1}]
$\dot{m}_t$	=	Total mass flowrate [kg s^{-1}]
P_{t0}	=	Total pressure at station 0 [kPa]
P_{02}	=	Total pressure at station 2 [kPa]
P_{02B}	=	Total pressure at station 21 [kPa]
P_{02C}	=	Total pressure at station 25 [kPa]
P_{03}	=	Total pressure at station 3 [kPa]
P_{04}	=	Total pressure at station 4 [kPa]
P_{4A0}	=	Total pressure at station 44 [kPa]
P_{05}	=	Total pressure at station 5 [kPa]
R	=	Ideal gas constant [J [kg K]$^{-1}$]
Re_t	=	Turbulent Reynolds number
S_a	=	Stoichiometric ratio

S_L^0 = Unstretched laminar flame displacement speed [m s^{-1}]

T_c = Engine thrust at cruise (N)

T_{t0} = Total temperature at station 0 [K]

T_{02} = Total temperature at station 2 [K]

T_{02B} = Total temperature at station 21 [K]

T_{02C} = Total temperature at station 25 [K]

T_{03} = Total temperature at station 3 [K]

T_{04} = Total temperature at station 4 [K]

T_{4A0} = Total temperature at station 44 [K]

T_{05} = Total temperature at station 5 [K]

u' = Turbulent fluctuation of bulk flow velocity [m s^{-1}]

V_a = Aircraft cruise velocity [m/s]

V_{EB} = Bypass stream exhaust flow velocity [m s^{-1}]

V_{EC} = Bypass stream exhaust flow velocity [m s^{-1}]

α = Air flow split ratio

β = Engine bypass ratio

δ = Diffusive laminar flame thickness [m]

η_i = Inlet diffuser efficiency

η_f = Fan efficiency

η_{hpc} = High-pressure compressor efficiency

η_{lpc} = Low-pressure compressor efficiency

η_n = Nozzle efficiency

η_{tur} = Turbine efficiency

η_k = Kolmogorov turbulence scale [m]

γ = Heat capacity ratio

μ = Dynamic fluid viscosity [Pa s]

ν = Kinematic fluid viscosity [m^2 s^{-1}]

ϕ = Equivalence ratio

ϕ_g = Global equivalence ratio

π_b = Combustor pressure ratio

π_c	=	Overall pressure ratio [OPR]
π_d	=	Diffuser pressure ratio
π_f	=	Fan pressure ratio
π_{hpc}	=	High-pressure compressor ratio
π_{lpc}	=	Low-pressure compressor ratio
π_n	=	Nozzle pressure ratio
ρ	=	Density [kg m^{-3}]
z	=	Mixture fraction
χ_c	=	Scalar dissipation rate [s^{-1}]
$\dot{\omega}_k$	=	Species mass reaction rate [kg m^{-3} s^{-1}]
$\dot{m}_f$	=	Mass flowrate of fuel [kg s^{-1}]
$\dot{m}_a$	=	Mass flowrate of air [kg s^{-1}]
Y_k	=	Mass fraction of species k
f_s	=	Shielding function
S_l^0	=	Laminar unstretched flame speed [m s^{-1}]
S_t	=	Turbulent flame speed [m s^{-1}]
$h_{t,k}$	=	Total enthalpy of a particular species [J kg^{-1}]
c_p	=	Specific heat at constant pressure [J [kg K]$^{-1}$]
T_m	=	Mixture temperature [K]
s_a	=	Stoichiometric ratio
λ	=	Thermal conductivity [W [m K]$^{-1}$]
τ_{ij}^{SBES}	=	Viscous stress tensor for SBES model [N m^{-2}]
τ_{ij}^{RANS}	=	Viscous stress tensor for RANS model [N m^{-2}]
τ_{ij}^{LES}	=	Viscouss stress tensor for LES model [N m^{-2}]
ν_{ij}^{SBES}	=	Turbulent eddy viscosity for SBES model [$m^2 s^{-1}$]
ν_{ij}^{RANS}	=	Turbulent eddy viscosity for RANS model [$m^2 s^{-1}$]
ν_{ij}^{LES}	=	Turbulent eddy viscosity for LES model [$m^2 s^{-1}$]

Introduction

Scope of Thesis

The specific outline for the parts of this thesis is now discussed. Chapter one introduces the following topics: turbofan engines, performance modeling, flame flashback, and relevant prior works and state of the art. Two primary resources are used for the turbofan description, Ref. [1] and Ref. [2]. These two books give an overview of the turbofan engine and its operating principles. For combustion processes and flame stabilization, Ref. [3] is used alongside other textbooks and other published papers. The second chapter describes the modeling of a turbofan engine in Matlab with model validation in the turbomachinery software GasTurb. Mimicking the combustion conditions of a turbofan engine at cruising altitude in a ground facility are also presented. Chapter three discusses the computational fluid dynamic modeling of a laboratory scale burner with a focus on the combustion aspects in a lean hydrogen-air swirling flow system. Details on the meshing methodology with a review of the applicable models is also found there. The conclusion of the work is presented at the end and future aspects of this research is discussed.

Turbofan Engines Review

From internal combustion engines to turbojet engines to rocket engines, there exists several engine types in the world for various applications. One of the most popular types of transportation, air travel, is achieved via the gas turbine engine which exists in many forms. Gas turbine engines can be classified as turbojets, mixed flow turbofans, low bypass turbofans

and high bypass turbofans depending on engine design. Every type of aeroengine mentioned previously has a unique application that it is best suited for. Each category of gas turbine engines are also comprised of several sub categories for further classification. An example of further sub-classification of gas turbine engines would be augmentation with an afterburner. The addition of an afterburner to an aeroengine would increase the thrust output at the cost of fuel efficiency. In this study, the focus will be on a high bypass ratio, two spool turbofan engine with no augmentation.

High bypass turbofan engines are commonly used for civilian airliners and in cargo transport. This is because of their high fuel efficiency and ability to carry heavy payloads over long distances. Most high bypass turbofan engines can be identified from the prominent fan at the engine inlet, large nacelle and position under the wing of an aircraft. Famous aircraft using high bypass turbofan engines would be the C-5 Galaxy, Boeing 777, and the Airbus A321 which can be seen in Fig 1. These aircraft are supplied with aeroengines from a variety of manufacturers. Famous aeroengine manufacturers include: Rolls Royce, Safran, Pratt and Whitney, and finally General Electric. The demand for improving a turbofan engine's performance is higher than ever for the market. Several industry, government and academic research programs are currently working to address the many challenges and meet the demand. The drivers of the demand are: reduced operating cost, emission reduction, longer engine lifespan and improving power output. To meet this demand it is important to understand the characteristics of each engine component to maximize the current engine's performance and innovate for future aeroengines.

Figure 1: Airbus A321neo with high bypass turbofan engines [4].

The turbofan engine can be divided into stations, and each station is designated with a unique number and symbolizes a key module of the engine. Gas properties such as temperature or pressure are typically reported at the station numbers. Derived equations also use the station numbers to show how components are connected to one another. Most station numbering systems in academia and industry are somewhat similar to each other but have differences in naming conventions. American Institute of Aeronautics and Astronautics (AIAA) and GasTurb differences in station numbering can be seen in Fig. 2, and 4. In chapter two the station numbering is identified and described for a hypothetical high bypass turbofan engine.

Many power generation techniques and propulsion methods are based on thermodynamic cycles. Otto and Diesel cycles serve as the basis for automotive engines. Stirling engines are used for refrigerated engines or heat pumps. Power plants that use nuclear reactors are based on the Rankine cycle. In the case of aircraft, turbojet or turbofan, the cycle used is the Brayton cycle. The Brayton cycle describes the thermodynamic transformations that a fluid experiences through the engine's components. The Brayton cycle exists in many variations, the present case uses the standard Brayton cycle with no augmentation to the cycle. Each major engine component from the front of the engine to the rear of the engine can be mapped on the Brayton cycle. A standard ideal Brayton cycle is displayed on a temperature-entropy (T-S) diagram in Fig. 3.

The next central aspect of propulsion is the thrust from the engine. Thrust is a force generated by an aircraft's engine via acceleration of gases to propel the aircraft forward. Thrust in a high bypass turbofan engine is generated by applying a small velocity increase to a large amount of air passing through the fan. This is why high bypass turbofan engines are the most efficient type of gas turbine engines. An aircraft's engine also has to produce high thrust to overcome the drag generated from the surface body of the aircraft. There are many equations that show how thrust is created in a turbofan engine [1]. One of the forms of the governing thrust equation can be seen in Eq. 1.

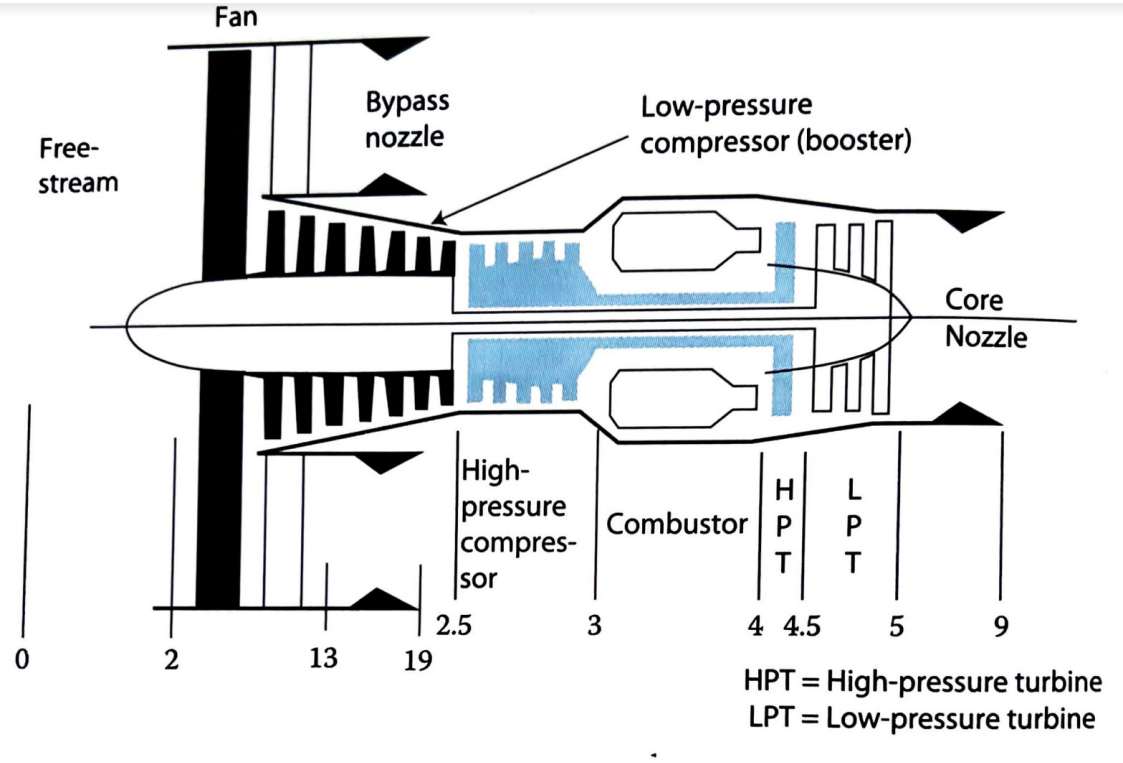

Figure 2: AIAA Standard high bypass turbofan station numbering from [1].

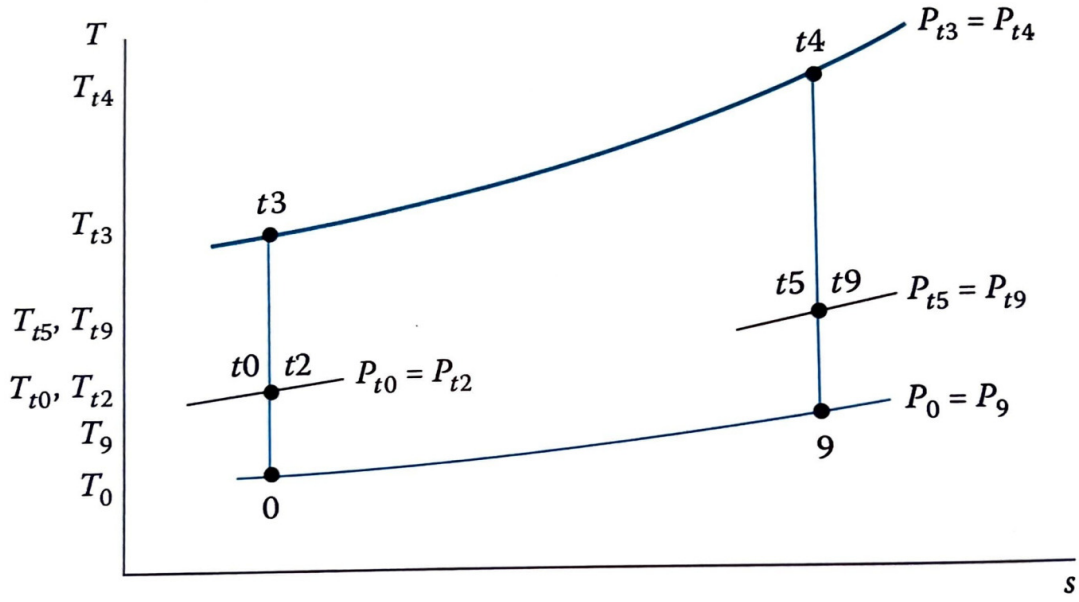

Figure 3: Standard ideal Brayton cycle with corresponding AIAA station location [1].

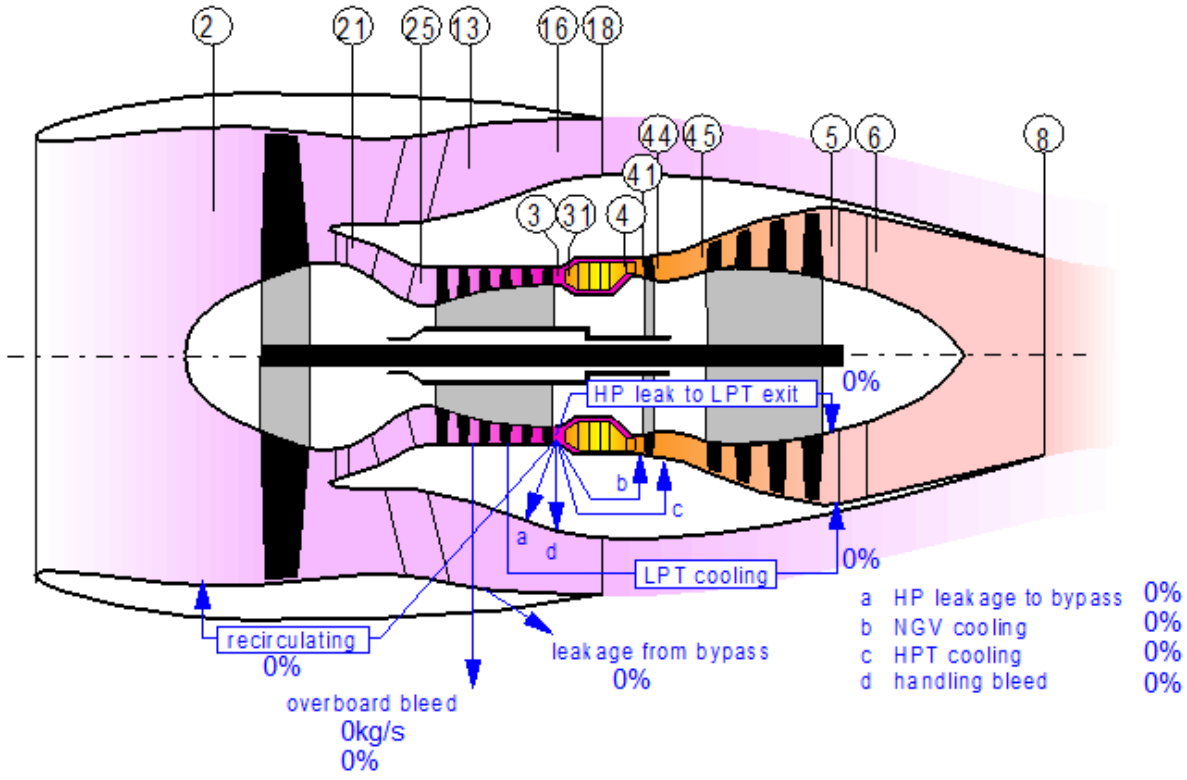

Figure 4: GasTurb high bypass turbofan station numbering [5].

$$F = \dot{m}_{core} \times (V_9 - V_0) + \dot{m}_B \times (V_{19} - V_0) \tag{1}$$

In Eq. 1 F is the installed thrust, and $\dot{m}_B$ is the mass flow rate of air through the bypass stream of the engine, $\dot{m}_{core}$ is the mass flow rate of air which flows into the core. The variable V_0 is the velocity of the aircraft. V_{19} is the velocity measured at the bypass stream exit and V_9 is the exit velocity of the core stream. Equation 1 subscripts corresponds with Fig. 2.

The path that a fluid takes through an engine is now described in general terms. Further details of each station and process will be provided in the appropriate sections. Using Fig. 2 and Eq 1, the flow path can be seen and described for an aircraft.

In a turbofan engine, atmospheric air first enters a diffuser. The role of the diffuser is to raise the total pressure of the flow by slowing it down. Slowing the flow down will help maximize the pressure which will increase thrust output. The fan is found at the end of the diffuser. The fan imparts a higher pressure on the flow further adding to the overall pressure ratio and total thrust. After the fan, the flow splits into the core flow and the bypass flow. The bypass flow passes through the converging nozzle and out of the engine into the surrounding atmosphere. The core flow passes to the low pressure compressor. The low pressure compressor (LPC) and high pressure compressor (HPC) increase the pressure by increasing the density of air. Fuel is then added to the air via injectors and brought into the combustor. The fuel air mixture is then ignited and the chemical energy of the mixture is now converted to thermal and kinetic energy. The next stage is the high pressure and low turbine stages (HPT and LPT respectively). The role of the turbines is to harvest the kinetic energy to drive shafts connected to the HPC, LPC and fan. After those stages the flow gains velocity by passing through a exhaust nozzle and exits to the atmosphere creating thrust. This process can be modeled with the First Law of Thermodynamics [6] shown as Eq 2.

$$\dot{Q}_{cv} - \dot{W}_{cv} = \sum_i [\dot{m}_i \times (h_i + \frac{V_i^2}{2} + g z_i)] - \sum_e [\dot{m}_e \times (h_e + \frac{V_e^2}{2} + g z_e)] \tag{2}$$

In Eq. 2, $\dot{Q}$ is the rate of heat transfer, $\dot{W}$ is the work rate, $\dot{m}$ is the mass flowrate, h is the enthalpy, V is the fluid velocity, g is the gravitational constant, and z is the height term. The lower case i indicates an inlet to a control volume while the lowercase e denotes the control volume exit.

Performance Modeling of Turbofan Engines

A Parametric cycle analysis is a subtype of a cycle analysis used to see how the thermodynamic properties of the working medium change in an engine when parameters are varied. Temperatures, pressures, bulk velocities, and fuel to air ratio can be tracked with cycle analysis. The performance analysis also investigates the turbomachinery aspects such as the compressor, turbine, and combustor design. The overall goal is to efficiently obtain the effects of how different engine designs change the overall performance of the engine. The data generated can then build stability and performance maps for the engine's specific components such as the compressor or turbines. More details are given in Chapter 2 about the parametric cycle analysis used in this work. Many of these analysis use specialized software such as Numerical Propulsion System Simulation (NPSS) [7], GasTurb [5] or many others. In this work, GasTurb is chosen and compared to a custom Matlab code developed and implemented in this thesis.

Flashback and Flame Stabilization

The purpose of combustion in a turbofan engine is to take the chemical energy of the fuel-air mixture and to convert it into thermal and kinetic energy. To study combustion and flame stability in this process, we must study combustion and flame dynamics with their underlying principles. For a flame to occur, three elements are required: a fuel source, an oxidizer, and an ignition source. Key phenomena of interest in unsteady combustion are flame flashback, flame blowout, flame blow off, and combustion instability. Flame flashback

in classical terms is where the flame front travels back against the fuel-air flow [3]. This can lead to unwanted combustion and severely damage the engine and components such as the injector. One cause of flame flashback is that the fuel air mixture is traveling at a lower flow speed than the flame is burning. When the flame speed is higher than the flow the flame travels back. Flame blowout occurs when the flame becomes separated from its fuel source and is pushed downstream by the flow [3]. Flame blow off is where the fuel or oxidizer source is reduced to a point where the flame can no longer sustain itself and is extinguished [3]. Elements of literature reviews on flashback and combustion are presented in chapter 2 and chapter 3 of this work.

Computational Simulation of Combustion

There are many tools available to study combustion in laboratory experiments, the list includes: laboratory burners, Schlieren [8], computational fluid dynamics (CFD) [9], Hydroxyl-Planar-Laser Induced-Fluorescence (OH-PLIF), chemiluminescence [10] and spectroscopy [11]. One major issue with gas turbine combustion and propulsion research is the high costs of conducting experiments. This is where CFD can be a valuable tool due to its ability to produce accurate results efficiently and at a lower cost than experiments. In general terms, CFD is a numerical method of modeling real world fluid or gas systems. CFD can be applied to a wide range of problems from pipe flows to combustion systems to hypersonic vehicles. It should be noted that CFD simulation and computer aided design (CAD) is used to aid experimentation and not replace it. For the simulations conducted in this thesis, the Ansys software package, particularly SpaceClaim, Ansys Meshing, and Ansys Fluent are chosen. Details about how the models, mesh, and simulations were developed are reviewed in the appropriate sections.

Hydrogen Large Scale Projects

Hydrogen as a fuel source for aviation has been considered in the past on several occasions by scientists and engineers [12]. It is important to review previous projects that investigated the use of hydrogen fuel for aviation purposes as they can offer insight into challenges faced today in modern hydrogen research programs. One interesting and noteworthy project using hydrogen for propulsion research was the NACA-USAF Bee Project. This project is discussed because the respective aircraft actually flew allowing us to see how a hydrogen powered aircraft behaves in real world flight conditions. Recently, hydrogen fuel has gained attention because of its ability to eliminate pollutants such as carbon dioxide (CO_2), eliminate soot, and increase overall fuel efficiency. These perks are attractive to engine manufacturers trying to reduce pollution and increase overall system efficiency.

The Bee Project

In 1955, the United States Air Force (USAF) and the National Advisory Committee for Aeronautics (NACA) began research into liquid hydrogen fuel for aircraft. The interest was on a high altitude subsonic reconnaissance aircraft. For this project, a subsonic bomber, subsonic reconnaissance aircraft, and supersonic fighter were also considered but the main focus was the subsonic reconnaissance aircraft [12].It was found that hydrogen could combust in a low pressure environment (*i.e.* high altitudes) where traditional jet fuels could not. To test the idea of hydrogen propulsion a readily available aircraft was required to serve as a prototype. The test aircraft selected was the twin engine Martin B-57B Canberra, a license built version of the British English Electric Canberra bomber. The B57-B seen in Fig. 5, was powered by two J-65 single spool, axial flow turbojets, one of which would be modified to run on both hydrogen and JP-4 kerosene [12]. The project goal was to evaluate hydrogen's potential as a fuel source and to study the changes in handling and performance characteristics of the engine. The research team modified and built only what was needed to get the engine working, in this case it was the hydrogen fuel system and flight control systems.

Hydrogen is a difficult fuel to store in a liquid form. Hydrogen's low density requires the use heavy insulated tanks which is prohibitive on an aircraft where every millimeter of space and kilogram counts. The hydrogen fuel system had two proposed pumping schemes to transfer the fuel from the tanks to the engine. The first plan was to pressurize the hydrogen tank with helium, a simple and fast method but requiring a heavy tank to withstand the pressure. The extra weight was not ideal and caused performance loss. The second idea was to use a liquid-hydrogen pump, which required development time which was limited. Therefore the first tests were made with the pressurization of the hydrogen tank with helium. The final wing tip tank was made from stainless steel.

The transition from JP-4 kerosene to hydrogen fuel is now described. From Ref. [12] "The dual fuel system and transition between the two fuels, JP-4 and gaseous hydrogen, called for an integrated control system, the key component of which was a flow regulator for the gaseous hydrogen. The speed of the engine was controlled by coupling the hydrogen flow regulator to the engine's JP-4 fuel control". To accomplish this, the fuel lines for hydrogen would need to be purged first. Then the engine would run on a Kerosene-Hydrogen mixture. After a certain amount of time had passed, the engine would operate fully with hydrogen fuel. No changes were made to the engine components in the B57-B such as the compressors, turbines, or combustor [12]. A hydrogen manifold and injection tubes were used but were checked to make sure that the JP-4 system was not compromised. To turn the liquid hydrogen into a gaseous form a heat exchanger with ram air was used [13]. A schematic of the heat exchanger can be seen in Fig. 6 with major components identified. Extensive ground testing was also done on all major components as well at Mach 0.8. After ground testing was complete, the plan was after flying to an altitude of roughly 16,000 meters the fuel source in one of the two turbojet engines would switch from JP-4 to hydrogen [12]. When the hydrogen fuel experiment was complete, the engine's fuel would be switched back to JP-4 and the B57-B would return to base under normal operating conditions.

Figure 5: Glenn L. Martin Aircraft Company B-57 Bomber, this is the license built version of the British English Electric Canberra bomber [12].

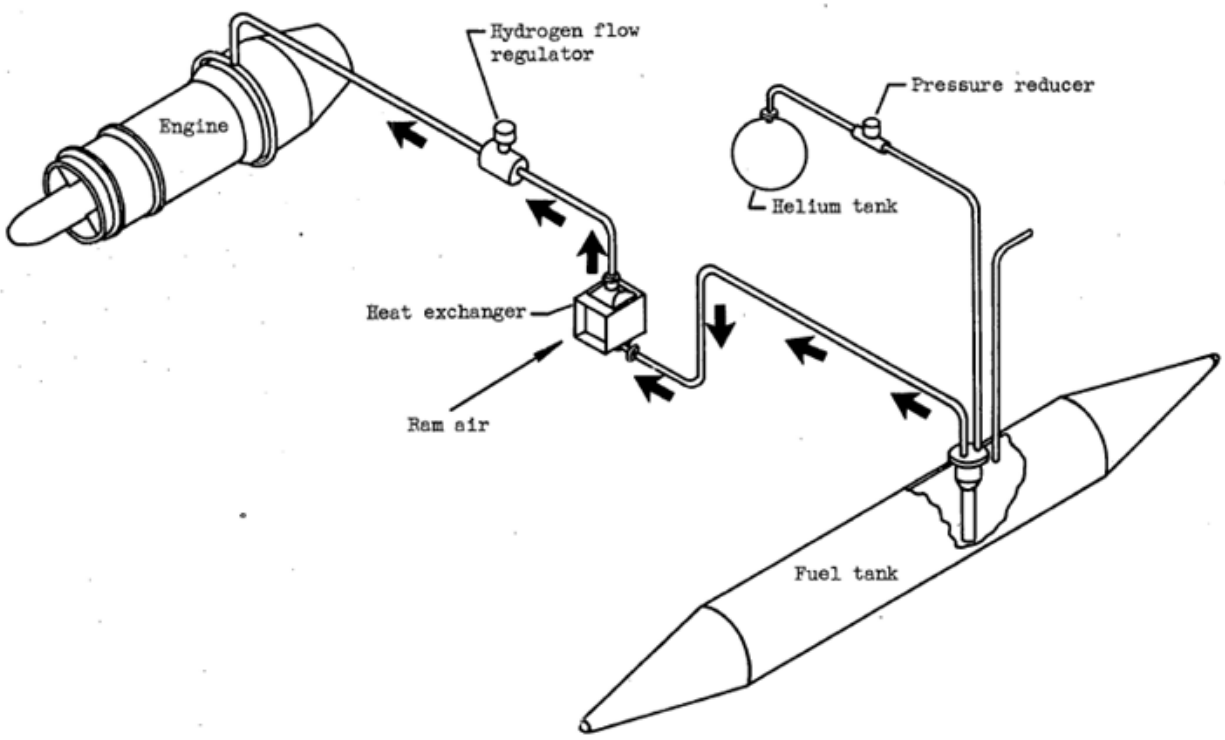

Figure 6: Heat exchanger scheme used in Project Bee [12]

Modern Programs

There are numerous industry programs investigating hydrogen as a potential fuel source. Rolls Royce is looking into hydrogen as an electrical source or a direct fuel source for small to medium sized aircraft with the H2ZERO and Net Zero programs [14]. Pratt and Whitney is investigating gas turbine engine designs that use liquid hydrogen fuel with water vapor recovery in the HySIITE program [15]. CFM International, a joint company split between General Electric and Safran Aircraft Engines, is re-configuring a General Electric turbofan engine to work with hydrogen fuel in the RISE program [16]. Airbus's program ZEROe is researching liquid hydrogen combustion and hydrogen fuel cells in retrofitted gas turbine engines [17]. These programs shows that the global community is greatly interested in hydrogen propulsion systems for aeroengines.

Chapter 1

Turbofan Engine to Lab-Scale

1.1 Disclosure Statement

This chapter originates from a published paper by the same author of this work Ref. [18]. The author of this thesis was the lead author of that work. The co-authors were: Dr. Palies, Mr. Prater, and Mr. Kolwyck. The paper was published in the American Institute of Aeronautics and Astronautics. This was presented in the SciTech Forum held in National Harbor, Maryland in 2023. Edits include formatting, syntax corrections, and details to help bridge this section with the following section.

1.2 Introduction

Hydrogen as a fuel source for a gas turbine engines, for both power and propulsion applications, has been considered for decades as the specific energy is high compared to other fuels and more recently as no carbon dioxide (CO_2) is generated. An additional benefit of hydrogen is that when properly premixed and in the lean combustion regime nitric oxide (NOx) production is drastically reduced. Several industry research programs are investigating hydrogen fuel for gas turbine propulsion. Pratt and Whitney, CFM, Rolls-Royce and Airbus are all assessing and working towards hydrogen propulsion with fuel cells or retrofitted engines. However, these programs are not primarly focused on premixed swirl-stabilized hydrogen-air combustion. There are many challenges to address before deploying

combustion systems operating with premixed hydrogen/air flames. In order to retrofit current gas turbine engines to work with hydrogen, there are three key aspects to research: the combustion processes and the combustor, the fuel distribution system, and the fuel tank. The first element is related to flame stabilization of hydrogen/air flames and is the focus of this work. In combustion processes there exists several challenges for both static and dynamics flame stability. Flashback and combustion instabilities are the key behaviors to study and the burner design presented in this section has the goal to provide a platform for capturing those phenomena as well as aid in the advancement in the base literature around premixed swirling flame stabilization.

Flame stabilization is a cornerstone aspect to combustion science because of its importance for gas turbine engines, rockets and other propulsion systems. The combustor design and combustion/flame process ignite the fuel-air mixture coverting the chemical energy into kinetic energy which can be harnessed by the engine. In aeroengines, the combustion system consists of a set of fuel injector units. Currently, modern turbofan engines mostly depend on swirling flames operating in diffusion or partially-premixed flame regimes with standard hydrocarbon fuels such as kerosene [3]. Future turbofan engines may operate in premixed regimes with hydrogen fuel. In that regard, flame stabilization studies are crucial to enable such combustion systems. The next sections in this chapter will re-situate this context within the referenced literature.

For premixed hydrogen-air flames, some studies in literature have shown flame stabilization with significant hydrogen content up to 100% full hydrogen, yet high swirl level cases are few. One of the closest examples is a low swirl premixed 100% H_2/Air flame stabilization that is studied in Ref.[19] on the Low Swirl Injector (LSI) system. The LSI burner has been explored with hydrogen fuel mixed into other fuels as well in [20, 21, 22], but little research has focused on 100% H_2/Air flame stabilization at high swirl and fully premixed. Several configurations of swirled injections [23, 24, 25, 26, 27, 28] different from the LSI have been studied for flame stabilization but none with 100% H_2 content at this time. In general, the case of high swirled flame has been considered with only moderate levels of hydrogen fuel [29] and with investigations focused on combustion instability [30] rather than flame stabilization.

There are many reasons as to why no high swirled premixed 100% hydrogen-air flames have been studied yet. The first reason is that flashback could become the governing factor on a combustor stability map and thus needs to be countered with unique techniques. Secondly, the base information about flame stabilization of a highly swirled flame must build on the current knowledge that relies on the inner recirculation zone (IRZ) of burnt gas for flame stability.

Flame lean blowout is triggered when the combustion system operates near the lean flammability limit for a specific fuel. Near flammability limits of premixed hydrogen-air flames have been investigated in several studies. It has been demonstrated that the thermo-diffusive effects can be critical for high hydrogen content [31] that exist in low Lewis number regime where preferential diffusion dominates [32, 33]. The present work will focus on regime where the turbulence is hypothesized to dominate the flowfield and thus its interaction with the hydrogen flame front. So, the unique cell structures at the flame front are more than likely not to appear. Mostly, the thermo-diffusive cells structures occur for premixed flames that operate in equivalence ratios ranging from $\Phi = 0.5$ to $\Phi = 0.3$. A regime where the flame thickness is the highest and the flame speed the lowest. This system will also be operating at an equivalence ratio of 0.6. This can be seen on a Borghi diagram. The operating point on the Borghi diagram will shift towards the upper left as the equivalence ratio reduces from $\Phi = 0.6$ to the lean regime. This is because integral turbulent scale and velocity fluctuation can be assumed identical [3]. This can be seen in Fig. 1.1 from Ref.[3]. Whereas the equivalence ratio is expected influence the flame stabilization, the specific regime of unstable heat diffusion is hypothesized to be heavily influenced by turbulence. Knowledge in how turbulence competes with the differential diffusion effects [34, 35] remains to be studied in highly swirled cases. Experiments are required to test this turbulence hypothesis and support building the knowledge of premixed flames under turbulent effects. In Ref. [36] it was demonstrated that for H_2/CO syngas the thermo-diffusive instability strongly influences the lean premixed syngas cellular flame structure due to high preferential diffusion effects under small turbulence levels at elevated pressures.

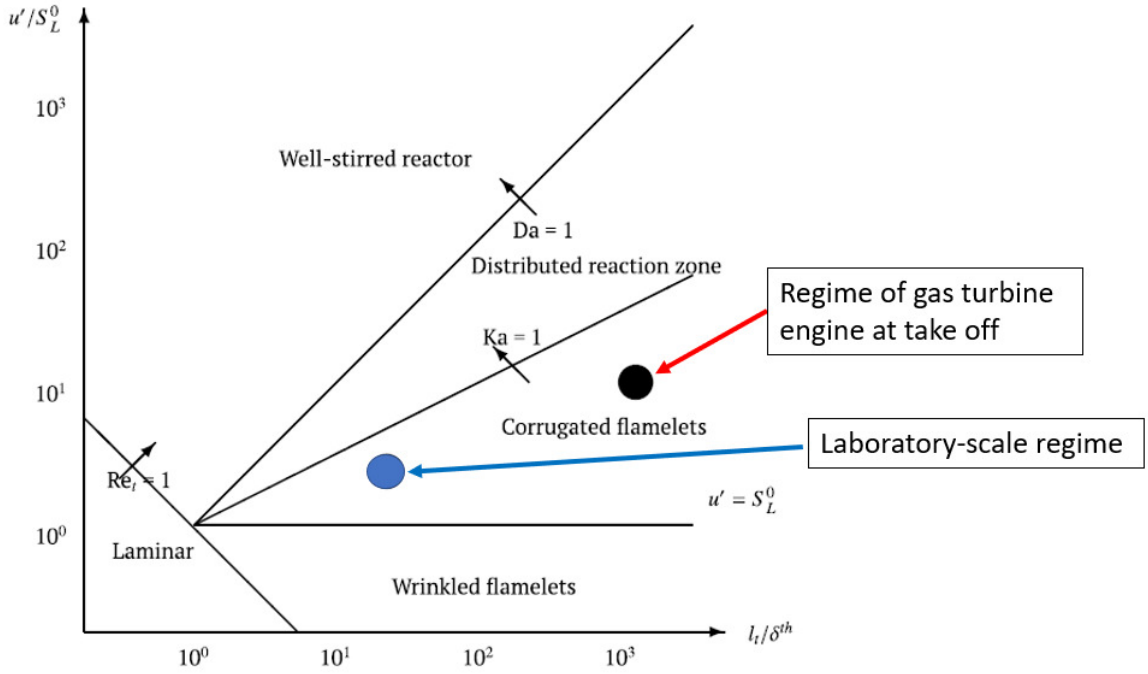

Figure 1.1: Borghi Diagram with operating points for the lab scale experiments and a turbofan engine identified [3].

The results from the study found that the thermo-diffusive effects are destabilizing and preferential diffusion is overwhelmed by turbulent mixing under high turbulence level at the elevated pressure [36]. Therefore, it is important to understand how the levels of turbulence affect the flame regime. This will also depend on the inlet axial flow velocity, system equivalence ratio, and the Lewis number. For the specific system presented in this work, lean blowout will not occur due to the equivalence ratio being outside of the lean flammability limit.

Flashback as discussed previously, is a combustion phenomena where a flame propagates back towards the fuel-air source. This is a safety concern for a premixed hydorgen-air combustor operating in a aeroengine. Several studies have been conducted on flame flashback for multiple injector configurations and fuel mixtures. In Ref. [10] the author investigated flashback with stratified hydrogen enriched natural gas flame for stationary gas turbine engine. Different mixtures ranging from 0% up to 90% hydrogen were used in the experiment. The swirl number for the system was calculated to be 0.9. Particle Image Velocimetry (PIV), chemiluminescence and Planar Laser Induced Florescence (PLIF) were the measurement techniques chosen for the experiment [10]. Chemiluminescence and PIV were used to study the transition to flashback whereas PLIF was used to study the equivalence ratio distribution in the injector mixing tube. Four distinct stages of transition to flashback were investigated. This work presented a detailed visualization of the flashback transition for hydrogen-rich flames.

Ref. [37] investigated with a reduced order model and experimental data the boundary layer flashback for a swirling, strained, and premixed flame. It was found that flashback occurs at the equivalence ratio where the strained extinction limit flame speed equals the mean axial flow velocity component at one thermal distance from the wall [37]. Two models were developed in the work, the first model used an experimentally measured wall velocity gradient while the second approach used simulated local near wall velocity [37]. However, the second approach required a correction factor due to the simulated near wall velocity being unresolved. The authors hypothesizes that Reynolds-Averaged Navier-Stokes Simulations

will be relevant to capture flashback because the model only depends on the mean flow velocity.

In Ref. [38], the authors investigated flashback with Direct Numerical Simulation (DNS) for a lean-swirled-premixed hydrogen-air combustor. Three dimensional simulations were conducted. The first simulation was modeling a stable hydrogen air flame at an equivalence ratio of 0.5 to establish a baseline flowfield. The second simulation was to analyze the flashback phenomena. Flashback was triggered by increasing the equivalence ratio from 0.5 to 0.8 and thus increasing the flame speed. When flashback occurred, two components of the flame were observed by the authors, a component referred as "flame tongue" following the main flow, and an other component propagating upstream and referred as "flame bulge" [38]. Initial results have found that the thermal condition of the bluff body plays a major role in the flashback phenomena [38]. In Ref. [38], flashback is investigated numerically with respect to the effect of the bluff body thermal condition. Both adiabatic and isothermal walls are applied. The mixture used consists of 95%-H_2-5%-CH_4 air flame. Two equivalence ratios were simulated: $\phi = 0.33$ for the stable burning baseline flame and $\phi = 0.4$ for the flashbacked flame. Two types of flashback are characterized: Mode 1 and Mode 2. A large scale swirling flame "tongue" is observed in flashback Mode 1 while flame "bulges" with no swirling motion is found in flashback Mode 2 [38]. The near wall flame flow interaction is also described. For these interactions, the distance between the flame tip ring and walls was studied [38] and reported to be important for flashback mitigation.

Combustion is a complex process with many sub-processes taking place at the same time. Heat transfer, thermodynamics, acoustics, two-phase flows, fluid mechanics, and chemical kinetics are interconnected to each other in what can be described as a synchronized system where one process changes the response of another and vice versa. It is important to understand this feedback loop since an instability can originate from any process. In a similar vein to flashback, combustion instabilities can lead to severe engine damage or massive downgrades in efficiency. There is a substantial amount of literature and research

on the subject of combustion instability but limited in the lean, high swirl, pure hydrogen regime area where this work pertains.

1.3 High Bypass Turbofan Modeling

Overview of Methods

In aerospace research, there exists several analytical or numerical methods that can be utilized for a turbofan design and analysis. Each method has its own assumptions, required inputs, conditions of application and calculation methods. Difficulties can be compounded if the engine considered is a modern engine with the majority of component specifications being considered proprietary information by the engine manufacturer. However, with these analytical or numerical methods on can estimate many parameters of an aeroengine which can then be used in subsequent calculations.

In order to replicate some of the key features of a turbofan engine combustor at the laboratory scale, an analysis is first conducted based on the propulsion performance of a turbofan engine. This turbomachinery analysis enables a calculation of the corresponding lab-scale combustion conditions. The engine chosen for this study is a modern high bypass ratio turbofan engine used for civilian airliners. The aircraft is assumed to be at an altitude of 11,000 m cruising at Mach 0.85 which is standard in the aviation community. Flow-field variables within the turbomachinery are reported using engine station numbers. The engine station numbers are defined points throughout the engine where calculations of gas properties are documented. Schematics and thermodynamic cycle diagrams are typically built upon those variables. This section introduces the thermodynamic-based parametric engine cycle analysis used to determine several engine properties at each of these stations including: operating pressure, temperatures, combustor conditions, and bulk flow velocities. Two gas turbine cases were conducted. One case with kerosene as the fuel and the second case using hydrogen fuel. The kerosene case was done first to establish a functioning code and comparison process. Once a process was established the fuel properties in the code

would be switched to hydrogen. The code was developed in such a manner that allows a user to interchange the type of fuel and turbomachinery properties with ease.

The thermodynamics-based performance analysis presented here was developed and implemented with specialized Matlab code, public domain aircraft specifications, documented turbomachinery properties, and governing equations applicable to an engine analysis such as Eq. 2. The estimated turbomachinery component properties such as efficiencies, pressure ratios, and bypass ratio originate from high bypass turbofan engines currently in use. The in-house code is developed and a validation of the results is made via a quantitative comparison with a commercial turbomachinery software called GasTurb. This comparison is done to determine if the in-house model of the turbofan engine can serve as a basis of a gas turbine engine performance analysis. The in-house Matlab model can also be coupled to additional models for both static (in development) and dynamic stability. This code can also be used to see how different component parameters change the overall performance of a given engine. The limited differences observed between the Matlab code and commercial software are also discussed and addressed. Figure 1.2 presents the resulting graphs showing the differences between the Matlab code and the commercial software at different points in the aeroengine. In Fig. 1.2a, the stagnation temperatures are plotted for both codes. In Fig. 1.2b, the stagnation pressures are plotted and compared to each other. A reasonable agreement is obtained between the Matlab model and the GasTurb software at all engine stations. It should be noted that in Fig. 1.2 ambient corresponds to atmospheric conditions from the International Standard Atmosphere. Inlet fan corresponds to downstream of the engine diffuser. LPC is the acronym of the Low-Pressure Compressor and HPC is the acronym of High-Performance Compressor. HPT stands for High-Pressure Turbine and LPT is the Low-Pressure Turbine.

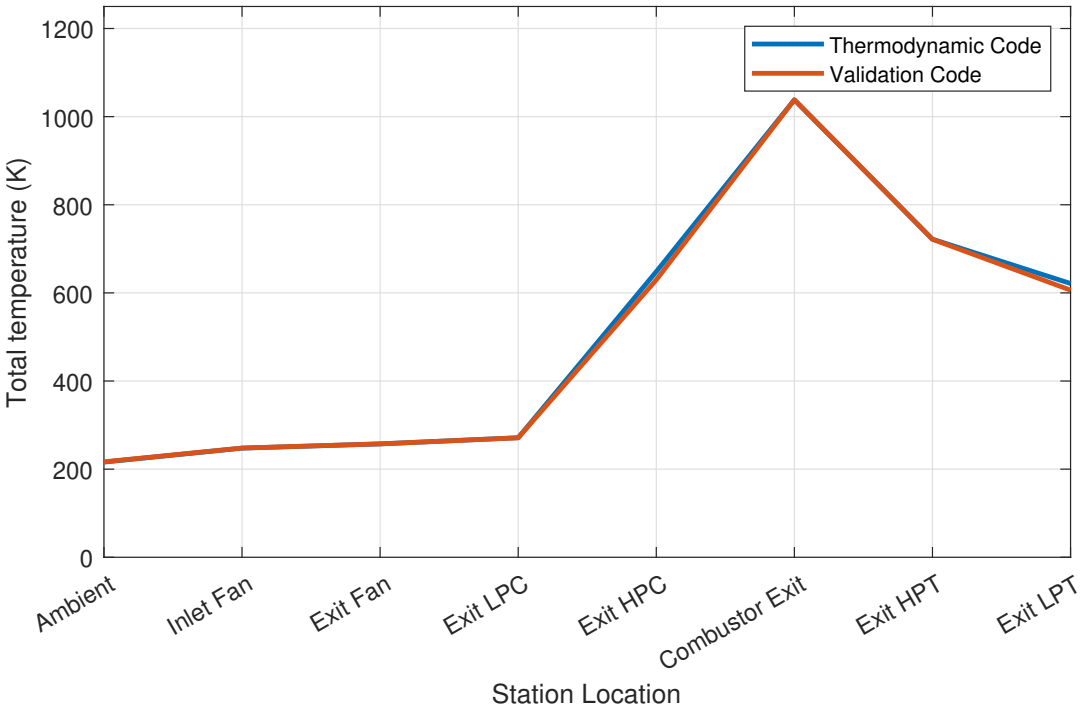

(a): Total temperatures inside of the turbofan engine

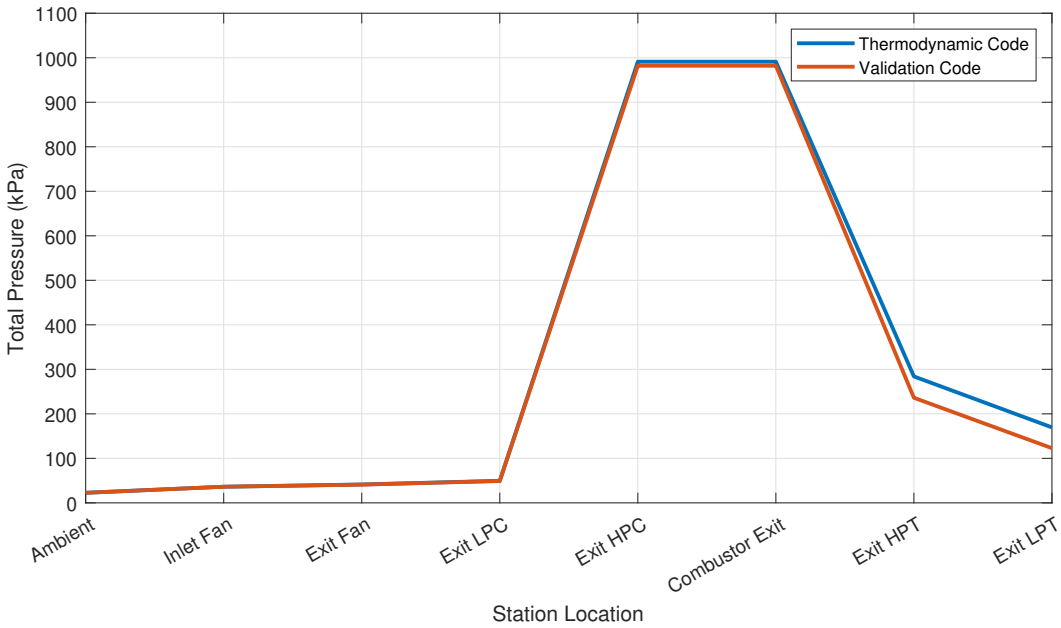

(b): Total Pressure inside of the turbofan engine

Figure 1.2: Total temperature (a) and Total pressure (b) for an hypothetical high-bypass turbofan engine operating with a hydrogen fuel source.

Aeroengine Engine Performance Model

The turbofan engine performance model is now detailed. The analysis determines engine performance characteristics based on a set of user inputs. Input values include atmospheric inlet temperature/pressure, compressor pressure ratios, aircraft velocity, and each component's mechanical efficiency. The following section outline the code developed and implemented [18]. The model requires first setting all known atmospheric and aircraft properties for the engine. Once the engine inlet and components are defined, one can progress throughout the turbomachinery to calculate both stagnation temperatures and pressures at each station in Fig. 2. With the Mach number at cruise, the atmospheric pressure and temperatures at 11 000 m altitude are known, one can compute the stagnation pressure at the engine diffuser upstream the fan:

$$P_{02} = P_a \times \left[\left(1 + \left(\frac{\gamma - 1}{2} \right) \times \eta_i \times M_a^2 \right)^{\frac{\gamma}{\gamma - 1}} \right] \tag{1.1}$$

One can compute also the stagnation temperature at the same location:

$$T_{02} = T_a \times \left(1 + \left(\frac{\gamma - 1}{2} \right) \times M_a^2 \right) \tag{1.2}$$

The next step is to proceed with the calculations for the rest of the defined stations throughout the turbofan engine. The stagnation variables downstream the fan of known pressure ratio can now be calculated. For the stagnation temperature, one obtains:

$$T_{02B} = T_{02} \times \pi_f^{\frac{\gamma - 1}{\gamma}} \tag{1.3}$$

For the stagnation pressure, one obtains:

$$P_{02B} = \pi_f \times P_{02} \tag{1.4}$$

The static pressure at station 2B downstream the fan is estimated to be equal to the ambient pressure and thus writes:

$$P_{2B} = P_a \tag{1.5}$$

Next, the outlet velocity at the fan can be solved for:

$$V_{EB} = \left[2 \times \eta_{ogv} \times \frac{\gamma}{\gamma - 1} \times R \times T_{02B} \times \left(1 - \left(\frac{P_{2B}}{P_{02B}}\right)^{\frac{(\gamma-1)}{\gamma}}\right)\right]^{1/2} \tag{1.6}$$

The variables are calculated with the following equations for the low-pressure compressor. The stagnation pressure writes:

$$P_{02C} = P_{02B} \times \pi_{LPC} \tag{1.7}$$

The stagnation temperature writes:

$$T_{02C} = T_{02B} \times \pi_{LPC}^{(\gamma-1)/\gamma} \tag{1.8}$$

For the high-pressure compressor, one obtains for the stagnation pressure:

$$P_{03} = P_{02C} \times \pi_{HPC} \tag{1.9}$$

And for the stagnation temperature:

$$T_{03} = T_{02C} \times \pi_{HPC}^{(\gamma-1)/\gamma} \tag{1.10}$$

The combustor variables are now solved for with the use of the following equations. The outlet combustor temperature writes:

$$T_{04} = \frac{(c_{p,c} \times T_{03} + \phi_g \times s_a \times hpr)}{(1 + \phi_g \times s_a) \times c_{p,h}} \tag{1.11}$$

The pressure is assumed to be slightly modified through the combustor:

$$P_{04} = P_{03} \times \pi_b \tag{1.12}$$

It is important to point out that the present analysis can be applied to any fuel used by aircraft today, the specifics for premixed combustor are not taken into account in this analysis

as only the turbine inlet temperature is used and not the adiabatic flame temperature. Future work at the Combustion Propulsion Aviation Research Center (C-PARC) will take those specifics into account [39]. The high-pressure turbine outlet stagnation values are next solved. For the temperature, one has:

$$T_{04A} = T_{04} - c_{p,c} \times \left(\frac{T_{03} - T_{02C}}{c_{p,h}} \right) \tag{1.13}$$

And for the pressure, one has:

$$P_{04A} = P_{04} \times \left(\frac{T_{04A}}{T_{04}} \right)^{\frac{\gamma}{\gamma-1}} \tag{1.14}$$

The low-pressure turbine outlet properties are now determined. For stagnation temperature, one has:

$$T_{05} = T_{04A} - \left(\frac{c_{p,c}}{c_{p,h}} \right) \times \left((T_{02C} - T_{02B}) + \beta \times (T_{02B} - T_{02}) \right) \tag{1.15}$$

And for the total pressure, one obtains:

$$P_{05} = P_{04A} \times \left(\frac{T_{05}}{T_{04A}} \right)^{\gamma/(\gamma-1)} \tag{1.16}$$

Finally, the engine outlet nozzle velocity can be found last with:

$$V_{EC} = \left[2 \times \eta_i \times \frac{\gamma}{\gamma - 1} \times R \times T_{05} \times \left(1 - \left(\frac{2P_a}{P_{05}} \right)^{\frac{(\gamma-1)}{\gamma}} \right) \right]^{1/2} \tag{1.17}$$

The thrust equation is now used to determined the engine core air mass flow rate. This leads to

$$\dot{m}_c = \frac{T_C}{[(1 + \phi_g s_a) \times V_{EC} - V_a) + \beta \times (V_{EB} - V_a)]} \tag{1.18}$$

Knowing the engine core air mass flowrate and because the bypass ratio β is 11, one can find the bypass air mass flowrate in the engine. This leads to:

$$\dot{m}_b = \dot{m}_c \times \beta \tag{1.19}$$

One can then deduced the required fuel flowrate with the definition of the FAR and the global equivalence ratio Φ_g:

$$\text{FAR} = \frac{\dot{m}_f}{\dot{m}_c} \tag{1.20}$$

The FAR can also write in terms of global equivalence ratio and stoichiometric ratio as:

$$\text{FAR} = \Phi_g \times s_a \tag{1.21}$$

It is then straightforward to determine the mass flowrate of fuel as:

$$\dot{m}_f = \dot{m}_c \times \Phi_g \times s_a \tag{1.22}$$

The total mass flowrate of air is the sum of the fan bypass air mass flowrate and the engine core air flowrate.

$$\dot{m}_t = \dot{m}_c + \dot{m}_b \tag{1.23}$$

These equations form the baseline Matlab code that was developed. The final results are compared to the commercial software Gasturb for validation.

Model Validation for Turbofan Engine

Once the script was developed, it required validation. This was done via the turbomachinery software GasTurb. GasTurb is a software designed to calculate and model different engine parameters at various stage on the flight envelope [5]. For the present validation study, the engine selected is a two spool unmixed flow turbofan. Thermodynamics based calculations are conducted because of the tractable number of parameters required as input. More advanced engine performance analysis can also be conducted to gather more comprehensive engine operating regimes including transient operation data. Design point analysis enables to find engine characteristics at any flight stage such as: takeoff, climb, cruise, decent, and landing. All inputs and outputs for the calculation are listed respectively in Tab. 1.1 and Tab. 1.2 for thoroughness and clarification purposes.

Table 1.1: Verification code values used for a high-bypass turbofan engine utilizing a hydrogen fuel source at a cruising altitude of 11,000 meters.

GasTurb Inputs				
Section	Input	Value	Units	Secondary Information
Basic Data	Intake Pressure Ratio	0.99*		* Indicates default value
	No (0) or Avg (1) Core dP/P	1*		
	Inner Fan Pressure Ratio	1.368		
	Outer Fan Pressure Ratio	1.14		
	HP Compr. Pressure Ratio	20		
	Bypass Duct Pressure Ratio	0.98*		
	Design Bypass Ratio	11		
	Burner Exit Temperature	1038	K	
	Fuel Heating Value	118.46	MJ/kg	"Hydrogen Fuel"
	Overboard Bleed	0*	kg/s	*This is for the secondary air system
	Power Offtake	0	kW	
	Burner Pressure Ratio	1		
	Mixer Efficiency	0.5		
Ambient Conditions	Altitude	11 000	m	
	Delta T from ISA	0*	K	
	Relative Humidity [%]	0*		
	Mach Number	0.8486		
Mass Flow Input**	Inlet Corr. Flow W2Rstd	iterated	kg/s	** W2Rstd given, "Fan Inlet Flow"
Efficiency and Design	LPC Efficiency	Isentropic : 1		
	LPC Design	no		
	HPC Efficiency	Isentropic : 1		
	HPC Design	no		
	HPT Efficiency	Isentropic : 1		
	LPT Efficiency	Isentropic : 1		
Nozzle Calculation: Standard	Nozzle Thrust Coefficient	1*		
	Bypass Nozzle Thrust Coeff	1*		
	Design Core Noxxle angle	10*	deg	
	Design Bypass Nozzle Angle	12*	deg	
Iteration Setup:	Inlet Corrected Flow	→		Thrust = 25 kN

Table 1.2: Comparison table between the Matlab code developed and the verification software GasTurb for the cruising hydrogen powered turbofan engine.

RESULTS COMPARISON FOR HYDROGEN FUEL						
	Engine Station	GasTurb Station	Location	Validation Results	Developed Code Results	% Difference
Total Temperature (K)	Ambient	Ambient	Ambient	216.65	216.00	0.30%
	T_02	2	Inlet Fan	247.92	247.66	0.10%
	T02B	13	Exit Fan	257.39	257.28	0.04%
	T02C	25	Exit LPC	271.18	271.29	0.04%
	T_03	3	Exit HPC	629.66	648.25	2.87%
	T_04	4	Exit Combustor	1038.20	1038.20	0.0%
	T4A0	44	Exit HPT	721.60	721.85	0.03%
	T_05	5	Exit LPT	606.25	621.31	2.42%
Total Pressure (kPa)	Ambient	Ambient	Ambient	22.63	22.63	0.00%
	P_02	2	Inlet Fan	36.26	36.23	0.09%
	P02B	13	Exit Fan	40.92	41.30	0.92%
	P02C	25	Exit LPC	49.10	49.56	0.92%
	P_03	3	Exit HPC	982.06	991.14	0.92%
	P_04	4	Exit Combustor	982.06	991.14	0.92%
	P4A0	44	Exit HPT	236.09	284.03	16.88%
	P_05	5	Exit LPT	122.89	169.57	27.53%
Other Variables	Stated Output	Target Variable	Fuel Mass Flowrate (kg/s)	0.14	0.16	16.60%
	Stated Input	Stated Output	Net Thrust (kN)	25.00	25.000	0.00%
	Initial Input	Stated Output	Overall Pressure Ratio	27.36	27.36	0.00%
	Stated Output	Wf/3	Fuel to Air Ratio	0.004024	0.0050	19.40%
	Stated Output	18+8	Total Mass Flow Rate (kg/s)	404.012	390.341	3.50%
	Stated Output	18	Bypass Mass Flowrate (kg/s)	370.222	357.81	3.47%
	Stated Output	3	Core Mass Flowrate (kg/s)	33.657	32.53	3.47%
	Initial Input	Calculated Output	Equivalence Ratio	0.139	0.172	19.42%
	Initial Input	Initial Input	Flight Mach Number	0.8490	0.8456	0.40%

Towards the future goal of retrofitting existing aircraft engines with hydrogen, both a hydrocarbon-fueled and a hydrogen-fueled engines were modeled separately. The hydrocarbon (kerosene) case was conducted first to form a baseline. This baseline is then used as a retrofit target for the hydrogen-fueled case. For the validation with the developed code, all inputs were kept identical with the validation software. It included component efficiencies, altitude, and aircraft mach number. The Matlab code developed was validated with Parametric Cycle Analysis (PCA) in GasTurb. The construction of the performance model is based on literature propulsion and thermodynamics references [1, 2, 6, 3]. A parametric cycle analysis is chosen due to its ability to show the effects of different engine parameters on the system's thermodynamics rapidly. The analysis determines engine performance characteristics based on what the user inputs. Input values can include temperatures, compressor pressure ratios, rotational shaft speeds, aircraft velocity, and each component's mechanical efficiency. This method is also used to see how different component configurations change the overall performance of the engine.

The validation results reported in Fig. 1.2 are in close agreement. There are differences allocated to the thermodynamics data used for the developed model. Indeed, contrarily to the validation tool, to date, the developed model uses constant specific heat γ, universal gas constant R, and cold/hot specific heat values at constant pressure only.

1.4 Matching Combustion Conditions Between Engine and Laboratory-scale Experiment

The calculated performance is aimed at determining appropriate and relevant lab-scale combustion conditions. The laboratory-scale combustor presented in this paper and designed for future experiments will serve as a bridge to replicate key characteristics of future retrofitted hydrogen combustion turbofan engine. The undertaken aircraft/engine performance calculations build the required relationships between lab and engine scale. The laboratory scale combustor allows for the study of the gas turbine combustion environment

in terms of flame stabilization. Flame stabilization of a premixed flame is expected to have a direct scaling between lab and realistic combustor environment based on the kinematic budget at the flame front. Consequently, the laboratory scale experiment will allow for the study of the underlying principles of swirling premixed flame and combustion behaviors. These principles and basic mechanisms understanding can then be deployed on real scale systems.

The first step is to link the turbofan engine and its operating condition to the laboratory scale experiment operating condition. This involves replicating combustion condition between the engine and the laboratory scale burner. The specific combustion condition that need to be matched is the kinematic flame budget. The equation for the budget is $\boldsymbol{w_s} = \boldsymbol{v} + S_d\boldsymbol{n}$, where $\boldsymbol{w_s}$ is the flame surface velocity, $\boldsymbol{v}$ is the flow velocity vector, S_d is the flame displacement velocity, and $\boldsymbol{n}$ is the normal vector [3]. This involves similar flame speed, flow speed and turbulent combustion regime. The first step is to thus determine equivalence ratio, flame speed, flow speed and both Karlovitz and Damköhler numbers for the engine. These quantities as well as those used to derive them are defined next. For the inputs, the integral turbulence length scale l_t is taken as 90% of the swirler diameter. The next input is the turbulence velocity fluctuation u' which is taken as 20% of the bulk flow velocity U_b. The kinematic viscosity along with other gas properties are obtained from Cantera. The required constant grid spacing to reasonably quantify the flame properties for the system was found to be one micrometer in the Cantera code.

For a equivalence ratio of 0.6, the starting reactants contained hydrogen at 1.2 moles, oxygen at one mole, and nitrogen at 3.76 moles. The overall H_2/Air lean chemical reaction writes:

$$2\,\phi\mathrm{H_2} + (\mathrm{O_2} + 3.76\,\mathrm{N_2}) \longrightarrow 2\,\phi\mathrm{H_2O} + (1\text{-}\phi)\mathrm{O_2} + 3.76\,\mathrm{N_2}$$

Starting with a integral length scale which is 90% of the internal swirler diameter.

$$l_t = 0.9 \times D \tag{1.24}$$

Flows in a gas turbine combustor are often turbulent for fuel atomization, mixing and flame stabilization [1, 3]. In order to describe how turbulence interacts with the flame front, a percentage of the bulk flow is treated as turbulent flow.

$$u' = 0.2 \times U_{bulk} \tag{1.25}$$

The kinematic viscosity is now calculated by taking the density of the fluid at the static pressure and static temperature and using the dynamic viscosity obtained from Cantera.

$$\nu = \frac{\mu}{\rho} \tag{1.26}$$

The velocity, length scale, and kinematic viscosity can now be used in the equation for Reynolds number. The flame displacement speed S_L and flame thickness δ are solved for in the Cantera code.

$$Re_t = \frac{u' \times l_t}{\nu} \tag{1.27}$$

The unstretched laminar flame displacement speed S_L^0 and the diffusive flame thickness δ are are extracted from the 1D flame Cantera simulations performed at the engine conditions with:

$$\delta = \frac{\lambda}{\rho \times c_p \times S_L^0} \tag{1.28}$$

The Kolmogorov scale, is defined as where the turbulent eddy dissipates [3], can now be found with:

$$\eta_k = l_t \times (Re_t)^{\frac{-3}{4}} \tag{1.29}$$

The Karlovitz number, the ratio of the chemical time scale to the Kolmogorov scale [3], is now solved for:

$$Ka = \left(\frac{\delta}{\eta_k}\right)^2 \tag{1.30}$$

The Damköhler number, which is defined to be the turbulence integral time scale to the chemical time scale [3] and can be solved using:

$$Da = \frac{l_t \times S_L^0}{u' \times \delta} \tag{1.31}$$

The Cantera calculations are then reported and compiled into a table where the results are compared to the GRI 3.0 chemical kinetics mechanism.

Prior to determining those quantities for the engine, one needs to introduce the combustor flow split α for the engine as well as a number of injectors in order to study an individual injector at the lab-scale. The flow split ratio is defined by the ratio of air mass flowrate through the injector and total air mass flowrate. The subsequent air mass flowrate through the dilution hole is defined with $1 - \alpha$. When α is unity, all the air goes through the flame. In practice, for a premixed combustor, only a portion goes through the flame. In this work the flow split ratio is taken to be 0.25 [40]. The equivalence ratio ϕ is 0.6 at this flow split for the engine with hydrogen/air premixing. The number of injectors of the engine is chosen to be 80 so that the current experimental burner geometry can be directly utilized. Other larger diameters of swirlers can be considered as well to reduce the total number of injectors in an engine. In order to determine the Karlovitz number and the flame displacement speed for the engines, definitions from Ref. [3] are used. The chemical kinetics software Cantera is used to perform 1D premixed flame calculations shown in the previous paragraph. The 1D numerical simulations do take into account the multi-component transport model, energy equation, and the Soret effect.

The engine condition and the matching combustion condition for the lab-scale experiment are documented in a table. This table contains the values of the Karlovitz number,

Damköhler number, turbulent Reynolds number, Kolmogorov scale, flame displacement speed, and the flame thicknesses. The engine conditions are matched by increasing the inlet temperature of the premixture in the experiment to enable similar combustion conditions. The air at the lab scale can be heated with the use of a heat exchanger before entering the burner. The pressure in the lab is taken to be atmospheric (101.325 kPa). It is important to note that only the hydrogen case is conducted here, no kerosene or SAF fuel calculations are reported here.

Table 2.3 demonstrates that the laboratory combustion condition will match a future hydrogen premixed gas turbine combustor for flame stabilization research.

1.5 Description of the Laboratory-Scale Experiment

Selected components of the laboratory-scale combustor are now described. The present swirl-stabilized combustor is an evolution of the experimental setup documented in Ref.[42]. The present design is an advanced version of the fully premixed swirl burner designed previously [42] for methane/air high swirled flames. This experimental setup includes unique features: (1) the water-cooled central rod and plenum for flashback mitigation, (2) the swirler with translation adjustable position for combustion instability mitigation, and (3) the modular design of the overall system which allows for different experiment configurations. The first design step was to generate the CAD model to serve as a basis for assembly, manufacturing and CFD simulations of the corresponding lab-scale experiment. The design of the burner is highly modular in nature allowing for many different experimental configurations. The schematic of the experimental combustor is shown in Fig. 1.3.

The experimental setup depicted in Fig. 1.3 can be seen in Fig. 1.4. and in Fig. 1.5. A quartz tube (not shown here) will enable observation of the flame region with optical diagnostics. Mass flowrate controllers will be installed in order to accurately prescribed the amount of air and fuel flowing into the system. A premixing unit will be located upstream the burner to premix the fuel and the air.

Table 1.3: Comparison between the laboratory scale and turbofan engine combustion conditions.

Case	Mechanism	Lab or Engine	Input Pressure (Pa)	Input Temperature (K)	Flame Thickness (m)	Flame Displacement Speed (m/s)	Kolmogorov Scale	Turbulent Reynolds Number	Karlovitz Number	Damkohler Number
Case 1	[41]	Lab	101325	500	8.22E-05	1.92	2.88E-05	6,064	2.2	35
Case 2	[41]	Engine	955560	625	1.16E-05	1.85	7.19E-06	38,534.	0.93	242
Case 3	gri30	Lab	101325	500	7.70E-05	2.19	3.07E-05	5,556	1.59	43
Case 4	gri30	Engine	955560	625	1.35E-05	1.68	7.57E-06	36,007	1.05	189

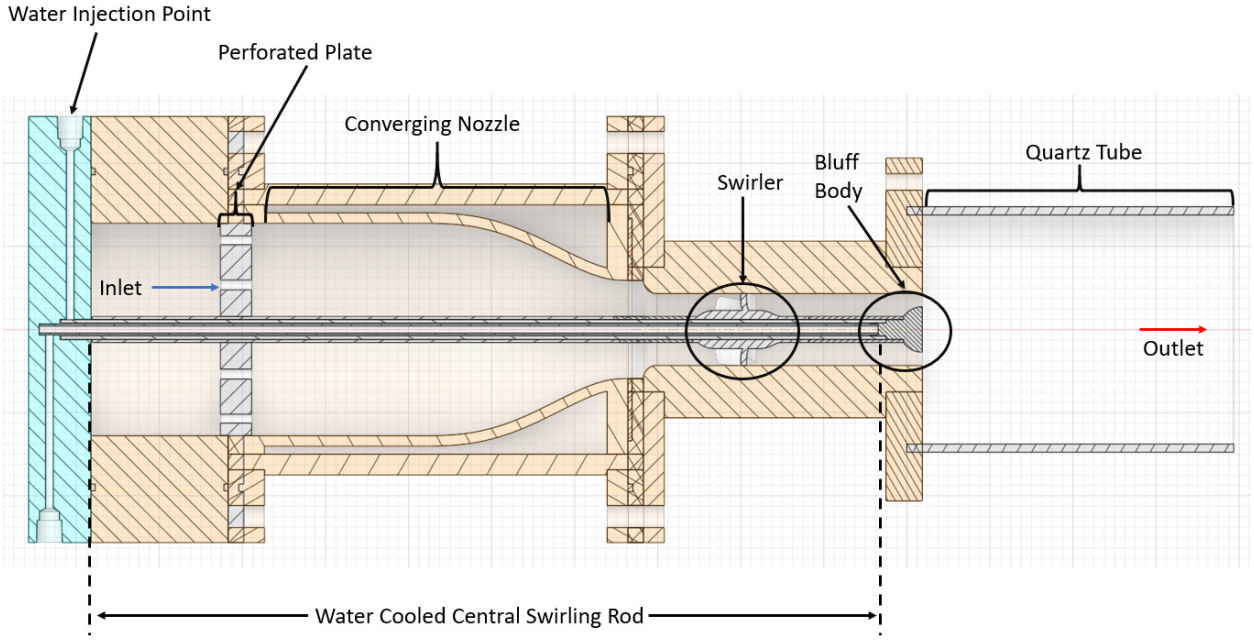

Figure 1.3: Section cut view of the burner with component identification. A perforated plate, the swirl vanes and central rod are identified for the reader. The quartz tube allows for optical measurements of the hydrogen flame using variety of techniques such as OH-PLIF and Schlieren.

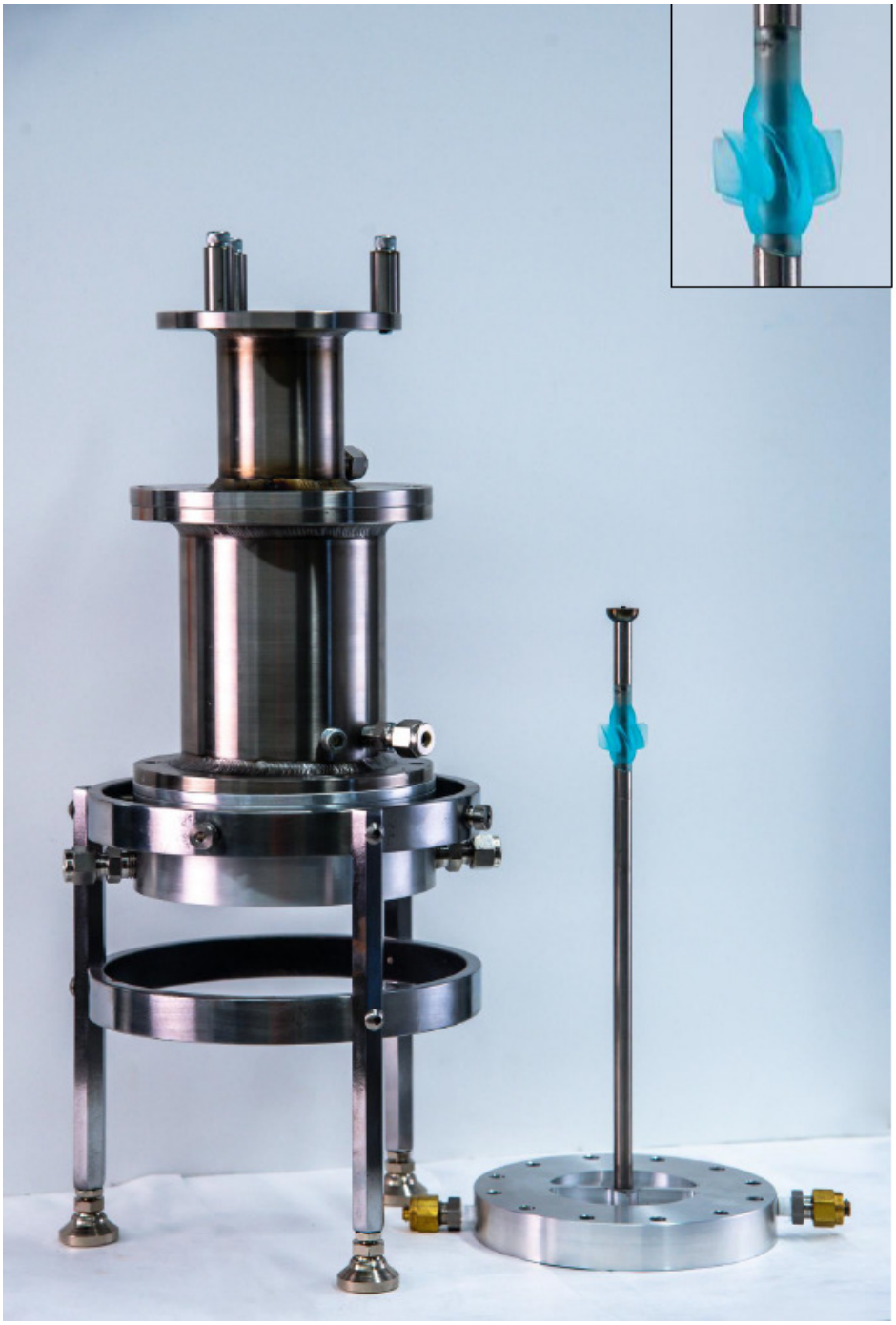

Figure 1.4: Partially assembled burner with the water cooled central rod and resin swirler shown on the side. The swirler is resin printed and consists of a series of airfoils. The central rod and the convergent upstream plenum are cooled via a cold water supply.

Figure 1.5: The four core parts of the burner are displayed. The top left image is the upstream plenum. The top right image shows where the quartz tube and flame will be anchored. The bottom left is the perforated plate located upstream the swirler. The bottom right is the burner stand with the with the perforated plate on top.

Two separate pipes will feed the base of the burner with the premixture formed. The option to inject fuel, air or premixed hydrogen-air at a variety of points also exist in this design. In order to capture the flame structures and potential dynamics, optical techniques such as Hydroxyl-Planar Laser Induced Florescence (OH-PLIF) or direct OH chemiluminescence with high speed cameras will be deployed. Both experimental and computational results will be compared. This will enable to both investigate flame stabilization mechanism and progress towards a robust full hydrogen combustor design.

Preliminary designs of the central rod tips (bluff bodies) are sketched in Fig. 1.6. These different design can be rapidly manufactured and efficiently tested for evaluation since a base aspect of the burner design is to be modular. Once the bluff body cap is in the CAD model a fluid volume can be generated then meshed. This mesh can then be used in a CFD simulation. The physical cap can be either machined via a mill, lathe, or by a metal 3D printer.

1.6 Non-Reacting Fluid Mechanic Simulations

The flow setup and internal fluid volume were defined to be the volume from the end of the perforated plate to the end of the quartz tube and is shown in Fig. 1.3. This flow volume was chosen to decrease the computational time and improve the efficiency of the calculation in the CFD solver. After the CAD model was completed in SolidWorks and imported into Ansys, a mesh was developed the model which can be seen in Fig. 1.7. The mesh itself contains nearly 13.2 million cells and 16.5 million nodes. The quality of the mesh was evaluated with a minimum orthogonal quality of 0.1 obtained. The mesh has a poly-hexcore structure designed using a maximum cell size of 0.01 inches for the fluid volume which can be seen in Fig. 1.7. The next step relied on conducting numerical simulations of the baseline flow on this burner configuration to assess the presence of swirling flow features such as the inner recirculation zone, outer recirculation zone and the swirling jet lengths. If these features are not present, then a redesign of the laboratory scale burner would be required.

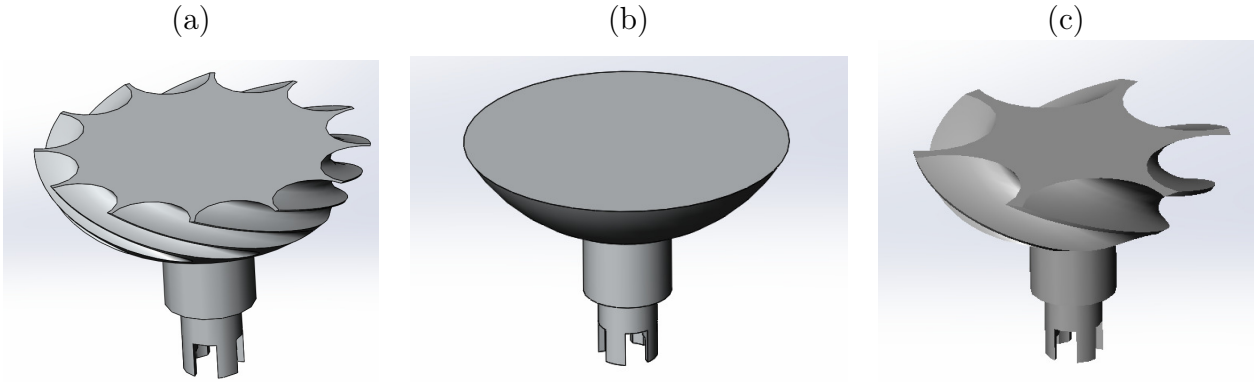

Figure 1.6: Concept rod caps designs. The core design of the central rod enables a variety of potential designs. (a) Design with 12 swirling channels carved into the sides of the cap. (b): This concept is based on the baseline design but with increased end diameter of the central rod cap. (c): Design with 6 carved channels similar to design (a).

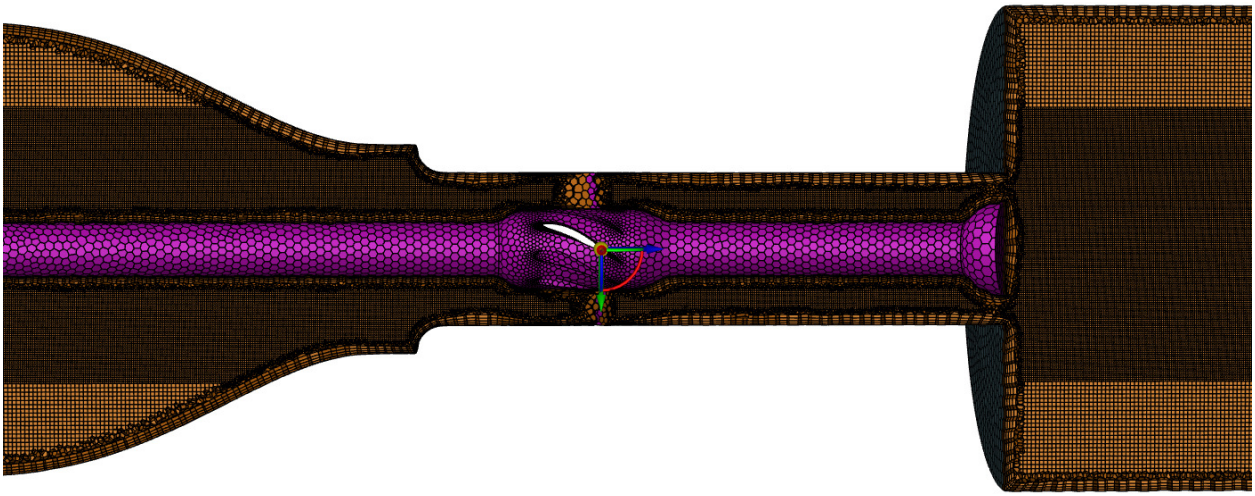

Figure 1.7: Cutaway view of the mosaic mesh structure.The flow path is from left to right. The end of the upstream plenum is first, followed by the swirler vane and then the central rod cap. The flame chamber is located after the cap. The purple rod in the center indicates a wall boundary.

The mesh has a poly-hexacore structure designed using the octree law where the maximum size is 2^n times the minimum size and can be seen in Fig. 1.7. The minimum size is 4.04 millimeters, which is the distance between the bluff body and wall, and n was chosen to be 3. The equation for the cell size writes max size $= 2^n \times$ min size. In Fig. 1.7 a region of highly refined cells can be seen along the central axis. This was done without the use of bodies of influence (BOIs).

The baseline non-reacting flow consists of atmospheric air and hydrogen at the appropriate inlet conditions. The air was modeled as an ideal gas. The computational model chosen for the non-reacting case was the RANS k-Omega two equation model allowing a calculation of the time averaged flow field. A mass flow inlet with a pressure outlet is selected for this experiment. A mass flow of 0.0150 (kg/s) is chosen at an inlet temperature of 500 K. The actual device will have mass flowrate meters controlling the flow from the tanks during experiments. The numerical scheme was set to coupled with the spatial discretization set to second order. Under relaxation values were left at the solver's default value. Residual monitors for the continuity equation and energy equation were reduced from 0.001 to 1e-06 to tighten the convergence parameters. The final setting was conducting a hybrid initialization for this case. Scaled residuals levels as well as the mass balance between the inlet and outlet of the burner are both used to confirm that the simulation results are converged. The scaled residuals converge after 500 iterations at 10^{-6} or below for all equations. The mass flow balance between the inlet and outlet of the system is $2.45e^{-13}$ (kg/s), a value very close to zero. Contours of the non-reacting flow can be seen in Fig. 1.8A, Fig. 1.8B, and Fig. 1.8C. Flow features such as the inner recirculation zone (IRZ), outer recirculation zone (ORZ), and the swirling jets can be seen in the contours of radial and tangential velocity. After a baseline flow has been established, a new reacting flow case for the combustor is made using a mixture of H_2 and air (O_2 + N_2). This new reacting field of the laboratory scale combustor will consist of hydrogen and air at a 0.6 equivalence ratio with a new set of boundary conditions in the next chapter.

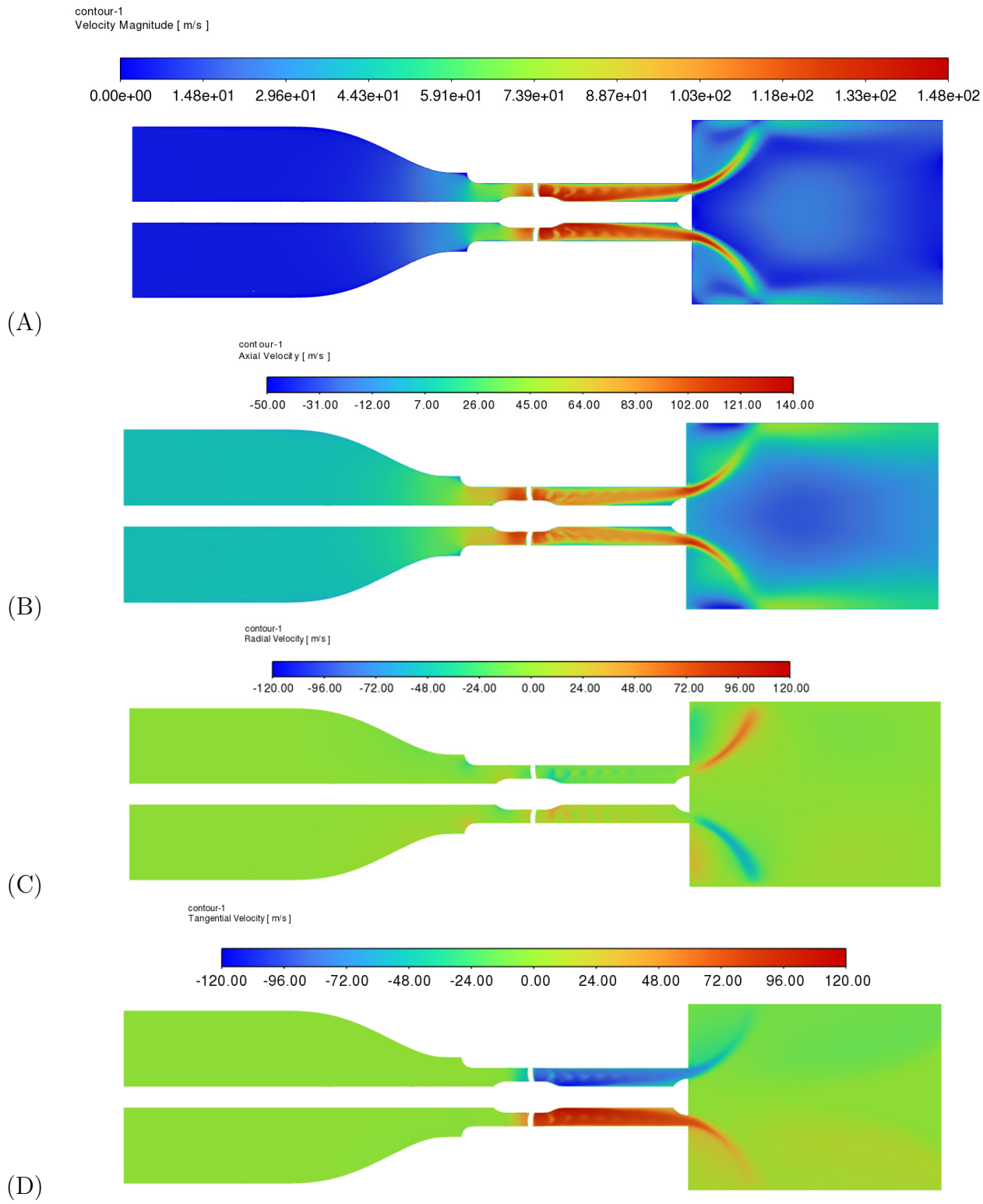

Figure 1.8: (A): Magnitude of the velocity components inside the burner. (B): Axial velocity component for the non-reacting field. (C): Radial velocity component. (D): Tangential velocity component.

1.7 Conclusion

In this section, a method for the development of a laboratory-scale combustor is presented. The method includes the determination of the relevant operating condition for the laboratory-scale setup in order to replicate the relevant combustion condition for a gas turbine aircraft engine. The method involves four major steps: (1) the calculation and the validation of the engine performance, (2) the determination of the combustion conditions at the laboratory-scale, (3) the design of the burner itself, and (4) numerical simulations at relevant conditions to observe key flow features of the targeted swirling flow. The first step of the method implies to use parametric cycle analysis of the turbofan engine with a developed code. The obtained results consist of fluid properties throughout the engine turbomachinery at the following stations: inlet, fan, compressors, combustor, turbines, engine outlet and fan bypass outlet. It includes temperatures, pressures, and velocities. The construction of the parametric cycle analysis is presented in the paper and is based on literature references. Specifics for premixed combustion are factored in with an additional parameter, the combustor flow split. Future work will coupled this performance analysis with a combustor performance map. Other quantities such as mass flow rates of fuel and air, exit velocities, and pressure ratios, are calculated as well. The results of the performance parametric cycle analysis are compared to a validation software. Results at each engine station for both the stagnation temperature and stagnation pressure are then compared. Percent differences tables between the developed code and the validation software indicate few percent difference for most variables at all stations and higher differences a few downstream station. These are discussed and attributed to assumption on heat capacity and specific heat ratio held constant. Next, it was also shown that the engine combustor will operate close to unity Karlovitz number turbulent combustion regime where the flamelet assumption is applicable. Based on flame budget kinematic, one expects that the laboratory-scale experiment will replicate both turbulent combustion regime as well as main bulk flow velocity that are critical for flame stabilization. The design of the burner consists of the geometry and special features (water-cooled central rod, translatable swirler, and highly modular design such as the central rod cap) described. From this geometry, the initial

computational mesh, and the simulation of the baseline non-reacting flow are conducted and presented. It is shown in the CFD contours that the IRZ, ORZ, and swirling jets are present.

Future work on the turbofan engine performance model includes transient analysis from takeoff to cruise including climb. This will allow for the study of realistic combustor conditions replicating some of the key features relevant to flame stabilization and combustion dynamics for those different flight regimes at the lab-scale condition. Future numerical simulations include reacting premixed case. The new reacting boundary conditions will serve as a initial test of the burner design. Then, the simulation results in chapter 3 are used to investigate flame stabilization by coupling the computed flow field with the kinematic balance at the flame front. This links the flame displacement speed, flow speed and flame surface speed [43, 44]. The flame kinematic budget will be used to track the flame position in the combustor and inform on the key relevant characteristic times at work for swirled flame stabilization. In addition, the presented experimental setup is being installed at UTSI allowing for experimental work to begin. These experiments will serve as a direct point of comparison for model validation

Chapter 2

Numerical Simulations of the Experiment

2.1 Disclosure Statements

This chapter is from [9] and will be published by the same author of this thesis in the American Society of Mechanical Engineers (ASME). The author of this thesis was the lead author of the paper. Co-authors include: Dr. Palies, Dr. Patil, Mr. Arguinzoni and Mr. Ansari. This paper will presented at the 2023 ASME Turbomachinery Conference held in Boston, Massachusetts. This work was conducted when the author was a summer graduate research intern at Ansys Inc. Edits include formatting, syntax corrections, and details reviewing the ignition process.

2.2 Introduction

The current knowledge gap in the literature for flame stabilization is on the mechanisms and process leading to or ensuring stabilization of 100% hydrogen/air lean premixed regime at high swirl and unity Karlovitz number. This regime typically presents a strong inner flow recirculation zone and a flamelet turbulent combustion regime. When studying swirling flame stabilization, laboratory scale experimental campaigns is a key step prior to scale up to more complex or even real scale gas turbine engine combustors. Indeed, due to their

modular design, and ease of observation of the flame behaviors as well as implementation of optical diagnostics, laboratory scale experiments are essential initial steps because they provides key insights into the relevant flow and flame processes.

Numerical simulations can be used to assess accurately combustor non-reacting flowfield features such as inner and outer recirculation zones in swirling flows as well as extent of the swirling flow jets. Computations can potentially guide on how sensitive a combustor design would be to flashback or combustion instabilities. Initial numerical simulations results presented in this article can provide a first validation step of the experimental design process for a particular design concept. Future experimental data can be then compared to computational results and confirm or not the design concepts assessed as well as support identifying model assumptions made and modeling strategies. The present work will also serve the long term goal of retrofitting a gas turbine engine with a premixed swirl stabilized hydrogen-air combustor.

Flashback into the injector unit of a combustor is the consequence of a flame stabilization that is not robust. Unknown processes and mechanism subsist to ensure such a robust flame stabilization in the regime considered here. Flashback has to be mitigated because its effect can affect the operating envelope of current and future combustion systems. Strategies based on flow and flame processes must be devised to remediate that challenge. Elements of the literature on flashback has identified several key features about swirling premixed flames. A wide range of basic mechanisms responsible for flashback have been identified and documented, see for example the recent book Ref.[45]. The base mechanistic phenomena was described in *Plee and Mellor*[46] as flashback occurring when the local flame speed value is higher than the local flow velocity such that the flame indeed propagates upstream its initial stabilized location. This is usually referred as *classical flashback*. Additional mechanisms include that of the *wall's boundary layer flashback* [47, 48, 49, 50, 51]. In a reacting swirling flow the *core flashback* is taking place in the center of the swirling flow field rather than on the wall's boundary layers. A variety of correlations have been examined [52, 53] and derived from data in the literature [54] to predict flashback. These have shown scaling versus

the tangential velocity of the flow or versus a formed Damköhler number. Much has been gained with the usage of high-speed diagnostics to investigate the dynamics of flashback and the transition from a stabilized position. Recent works have particularly focused on swirling premixed systems with hydrogen addition. For example, it has been found that flashback occurs primarily in the form of large-scale flame motion swirling in the bulk flow direction as they propagate upstream [48]. This finding should be explored further to determine if the driving motion of the flame during that transient is convection or thermal diffusion/reaction. Recent works have focused on [55] determining a practical condition where flashback is triggered. The flame front location was used as an estimate for flashback occurrence. The authors observed no flashback when the flame front base was located downstream of the mixing tube. However, the flame tip was always located upstream of the mixing tube outlet prior to flashback. It was concluded that the flame length to backplane height ratio was a sufficient condition for flashback occurrence. In other words, controlling the flame height on the centerline is a key aspect to consider. Some practical solution for flashback mitigation have been developed and include for example axial air injection on the center of the burner [56] or the use of micro-surface to control the boundary layer properties and thus the flashback [57]. In Ref.[50], the authors focused on comparing two methods to predict the minimum flow velocities to prevent flashback inside the boundary layer. The first one based on a Damköhler correlation fitted from experimental data at realistic gas turbine conditions but its applicability was limited to the turbulent combustion conditions of the initial data set. The second method was based on a flame angle approach based on a description of the physical process of boundary layer flashback including the local analysis of the onset of flashback for an assumed flame shape [58]. These two methods were combined to predict flashback occurence over a wide range of conditions bur are limited to one experimental setup. Additional works have focused on optimizing the injector shape and aerodynamic design of gas turbine combustors to avoid flashback phenomena [59]. It is recognized that there are no generally applicable aerodynamic design criteria for flame stabilization [60, 61]. Nevertheless, research works have attempted to contribute to the development of such design guidelines to reduce the need of excessive number of iterations of computational calculation to obtain the required velocity profile distribution and the vortex breakdown location [60].

Theoretical considerations have been undertaken in these studies to identify general rules and design criterion for flame stabilization. Whereas these studies are pioneering works, there are still a lack of a general swirl flame stabilization framework. Combustion induced vortex-breakdown (CIVB) is another mechanism that can lead to flame flashback which can occur only in premixed swirling flames without central rod [62]. The flame propagation is driven by the CIVB through the upstream mixing section occurring either during an increase of the equivalence ratio or a reduction of the mass flow rate. Flame flashback due to CIVB differs from the other mechanism because the heat release modifies strongly the flow field in the vortex core. The flame indeed shifts from it stabilized position to another one inside the injector.

CFD softwares are advanced tools recognized for fluid dynamics research and for design purposes. The use of Reynolds-Averaged-Navier-Stokes (RANS) and Large-Eddy-Simulations (LES) methods are standard in industry. Direct Numerical Simulations (DNS) is still not practical for design and is used for canonical configurations or specific case because of high CPU resources need. This section presents the initial results of a series of simulations that focus on the stabilization of a fully premixed swirled hydrogen-air flame. Section 3.3 presents the laboratory-scale experiment and design, Section 3.4 discusses the generated computational mesh, Section 3.5 presents the numerical models and boundary conditions. This is followed by the results for the non-reacting and reacting flowfield respectively. The obtained results including flow contours and flame shape are presented. The simulations include RANS, LES, and SBES. The software used is the ANSYS Fluent R2022 solver.

2.3 Laboratory Scale Experiment

The laboratory scale experiment is presented in this section. The burner is an evolution of the burner documented in Ref.[42]. This advanced version was conceived to model the fundamental mechanisms associated to swirling flame stabilization in 100% hydrogen/air lean premixed regime at high swirl and unity Karlovitz number. This experiment can be used to replicate some of the combustion conditions of a future turbofan engine

operating with hydrogen fuel in premixed combustor by satisfying the kinematic flame/flow speed budget and turbulence combustion regime. This experiment allows for the study of flame mechanisms and combustion phenomena such as flame flashback or combustor thermoacoustics for 100 % hydrogen/air lean premixed swirled flames. In Ref. [18], the connection between aeroengine combustor performance at cruise and laboratory scale experiment is made in terms of combustion conditions via the Karlovitz, the injector bulk velocity and the flame speed. This informs on the required operating condition of the laboratory scale burner to replicate the aeroengine combustor conditions at cruise for flame stabilization.

The numerical simulation settings and results in this chapter are for an initial case for the burner. DNS calculations will be conducted in a near future with additional codes. A semi assembled illustration of the burner and the complete computer aided design (CAD) drawing are shown in Fig. 2.1. This CAD model represents the fluid volume for the numerical simulations. The burner will be connected to a premixed unit where both fuel and air streams are mixed together and are controlled by mass flow meters. After being injected into the base of the burner the mixture flows past a perforated plate, and passes into the converging plenum. The flow is then set into rotation by the swirler. A central rod with a cap is on the centerline of the combustor. The flame is optically accessible into a quartz tube. The flame tube allows for laser diagnostics, Schlieren, flame chemiluminescence measurements, shadowgraphy, or other optical techniques for the swirl stabilized hydrogen flame. An outline of the experimental setup can be seen in Fig. 1.3. A summary of the design from chapter 2 is restated here. The perforated plate serves two purposes: control the turbulence fluctuations upstream the swirler, and control acoustics. Several plates can be manufactured and installed rapidly. The converging plenum accelerates the flow immediately before the swirler unit. The swirler is comprised of a series of resin 3D printed twisted blades equally spaced and radially distributed on the central rod. The swirler creates a swirling flow while the central rod cap serves as an additional anchor point for the flame. It is also worthwhile to note that the swirler on the central rod in the burner is translatable and the position can be adjusted for combustion instability mitigation. The burner is highly modular in nature to

(A): CAD Burner View

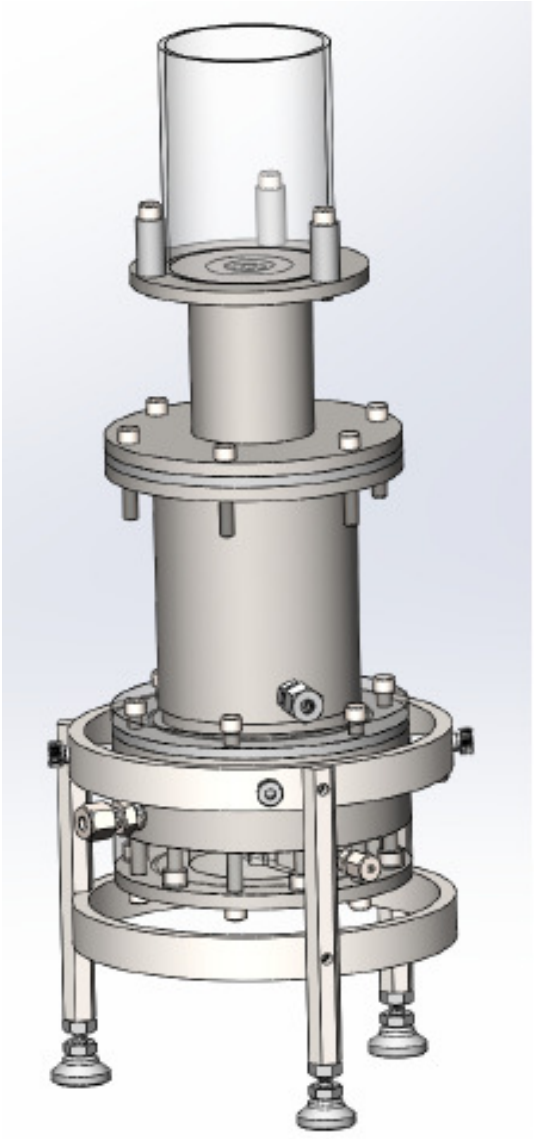

(B): Burner Photo

Figure 2.1: (A): 3D CAD rendering of experimental setup. (B) Semi-assembled experimental burner setup.

enable assessment of various geometrical modifications and thus effects of turbulence and acoustics for both flame stabilization and combustion instabilities. This allows for the study of hydrogen-air flame properties under different burner and combustion configurations.

A comparison between operating conditions for a premixed combustor and for the laboratory scale burner was conducted to set orders of magnitudes. Table 3.1 reports the final results and differences between the engine and lab scale conditions. For example, laboratory-scale combustors operate at atmospheric conditions (1 atm, 300 K) while turbofan engines operate at higher values (35 atm, 800 K) at take-off (TO) and (10 atm, 650 K) at cruise. This affects turbulence scales and combustion processes, specifically the turbulence dissipation Kolmogorov scale and the flame thicknesses scale. The estimated thermal flame front thickness at an equivalence ratio of 0.6 of a 1D laminar flame at atmospheric condition for hydrogen/air is of the order of 80 μm while it is of the order of 10 μm at the cruise condition [18]. Another comparison that needs to be mentioned is with respect to the combustor architecture. The laboratory scale uses a fully premixed combustion mode whereas current engine utilizes a Rich-Burn Quick-Mix Lean-Burn (RQL) architecture. Future combustors may be operating in Lean Fully Premixed Mode [63] and the present article contributes to this goal. Whereas turbulent combustion is important in future combustion systems applications as well as modeling and experimental capabilities [64], the regime of turbulent combustion is still subjected to discussion. Gas turbine combustors in real operating conditions in general raise questions and discussions in the literature on what are the appropriate regimes of premixed combustion.

Table 2.1: Comparison of engine and laboratory scale operating conditions.

Operating Conditions		
Variable	*Engine*	*Lab-Scale*
Altitude (m)	11,000 m	Sea-level
Fuel Type	Hydrogen	Hydrogen
Karlovitz Number	0.93	3.3
Damköhler Number	242	18
Injector Bulk Flow Velocity	65 m s^-1	25 m s^-1
Turbulent Reynolds Number	38,535	5,843
Equivalence Ratio	0.59	0.6
Oxidizer Type	Air	Air
Inlet Temperature	625 K	500 K
Thermal Power	19,488 kW	9 kW
Combustion Architecture	RQL	LFP
Fuel-Air Mixing	Diffusion/Partially Premixed	Fully Premixed

Ref. [65] have focused recently on attempting to characterize the highly turbulent premixed regime that may be at work in certain future combustion systems and pointed out that: *These findings indicate that the range of conditions for which flamelet models should be valid is larger than what was previously believed.* Work also focused on how to characterize these turbulent flames, and what are some of their macroscale behavior [66] at these relevant conditions. Analysis of realistic operating conditions also concluded to the relevance of the turbulent premixed flamelet regime in gas turbine engines [3]. These conclusions obtained are likely to hold for hydrogen/air flames where differential diffusion is likely dominated by turbulence effects. The present experimental setup will provide answers for confirming the turbulence combustion regime at work.

2.4 Computational Mesh

The grid generated for the baseline reacting and non-reacting simulations is described in this section. The software chosen for meshing is the Ansys Meshing package. The first step to generate the fluid volume from the CAD geometry to serve as a numerical domain is conducted via the CAD software SpaceClaim. Once the fluid volume is formed, the convergent plenum domain is reduced from its full length in order to not include the perforate plate modeling at this stage. This reduces the computing power required and improves the efficiency of the calculation. Essential features that affect the nature of the flow such as the swirler, central rod cap, and converging plenum are preserved. Once the this fluid volume was obtained, a mesh can be generated. The selected meshing strategy consists of ANSYS mosaic poly-hexcore mesh as it accelerates the meshing process with a reduced face count, higher quality cells and efficient parallel scalability. Mosaic meshing technology enables polyhedral connections between disparate mesh types. This meshing method uses octree hexes in the bulk regions, keeping an exceptional quality layered poly prism mesh in the boundary layer and connects the two meshes with basic polyhedral elements [67]. This mesh type allows for efficient and accurate results in a high range of simulation scenarios.

Several views of the resulting grid are seen in Fig. 2.2. The mesh has a poly-hexacore structure designed using the octree law where the maximum size is 2^n times the minimum size. The minimum cell volume size is 127 μm. n was set to 3. This leads to a maximum cell volume size of 1.016 mm in the mesh. Two cylindrical bodies of influence (BOI) are added to improve the mesh structure around the swirler, central rod cap, and quartz tube. BOIs are geometries that are used as part of the meshing strategy for improving the mesh structure by adding an arbitrary shape to the fluid volume which increases the mesh density around the given location. It should be noted that the use of a BOI does not interfere with the shape of the fluid volume or flow path of the fluid. The quality for the mesh is determined with both the LES mesh index and the orthogonal quality criterion. The LES mesh index is documented in Fig. 2.3 whereas the orthogonal quality was found to be 0.15. The orthogonal quality of a mesh is a common criteria used in CFD . Typically, values for the orthogonal quality greater than 0.1 are sought after during the meshing process [68]. This ensures the overall quality of the mesh. The orthogonal quality is defined by how uniform the mesh shape is [68]. Mesh orthogonal quality can be thought of as the inverse to cell skewness or how deformed a cell is [68]. In Fig. 2.3, the LES quality criterion derived from [69] is plotted with values from zero to one. Values greater than 0.8 and up to one indicate a meshed region is dense enough in terms of cell amount to allow for highly refined LES simulations and data collection in that area. The main area of interest, the combustion chamber, posses index values greater than 0.9. The swirler region is not fully resolved as shown with the index for the current simulation mesh. The region of the converging nozzle is not resolved either. While this does reduce measurement quality in that region the overall calculation efficiency improves. This strategy also reduces the total time it takes to generate the mesh. The total cell count of the mesh is 6.2 million cells. The poly-hexcore meshing method has been applied in a variety of combustion simulations. In one work by [69] a poly-hexcore methodology was used to study a CABRA flame's shear layer instabilities and mixing behavior. This affected the auto ignition and flame lift off in the simulation.

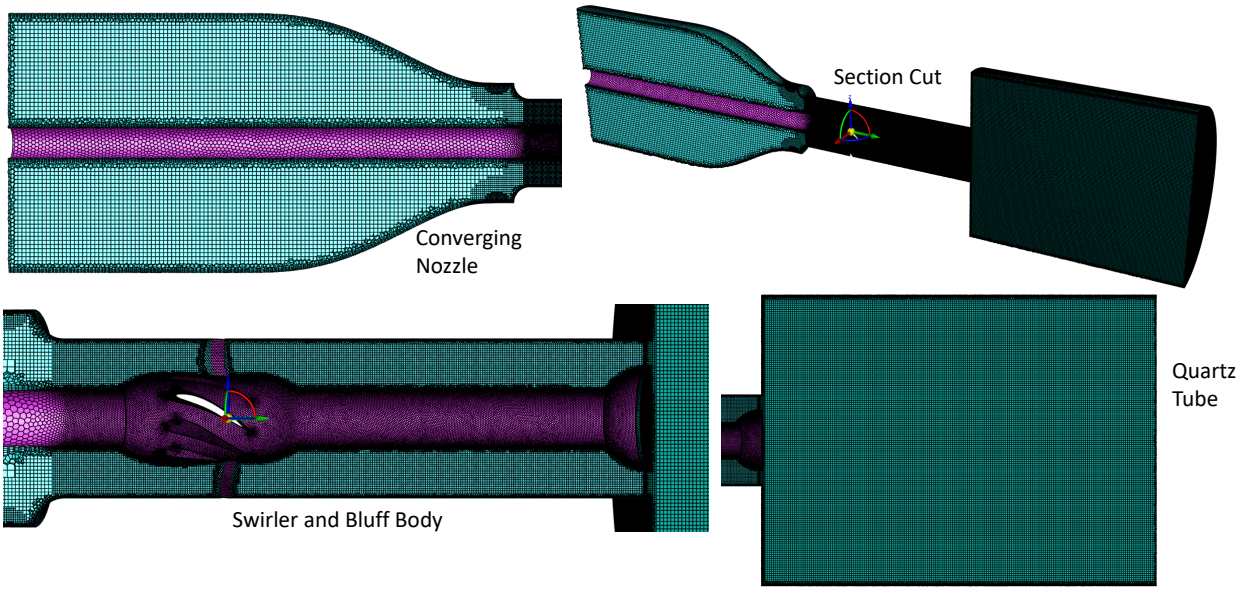

Figure 2.2: Zoomed in view of the mosaic poly-hexcore mesh (teal region) for the fluid volume of the burner. Top left image is the converging nozzle. Top right image is an isometric view of the mesh. The lower left picture is the swirler/central rod cap mesh. The bottom right image is the quartz tube mesh.

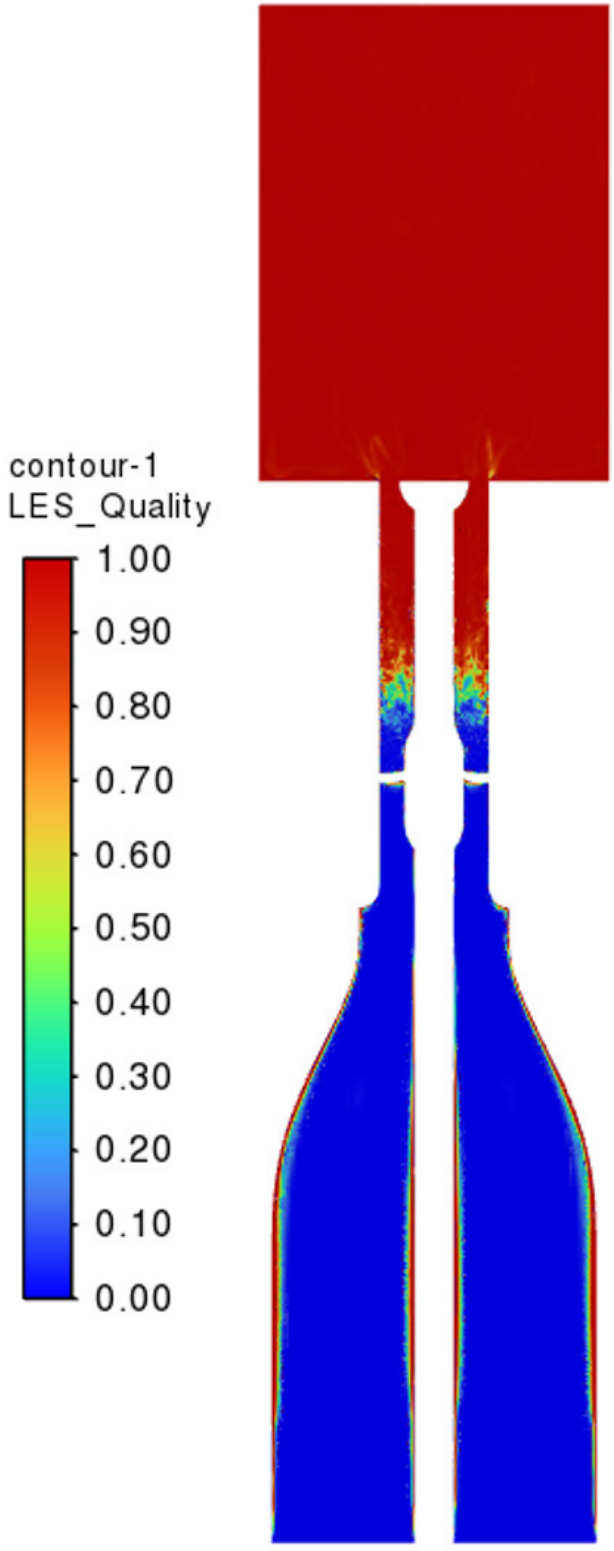

Figure 2.3: LES index of the mesh. Values close to 1 show a high quality region with a dense cell structure. Values closer to zero display a region that is not as refined.

Derivation of the LES Quality Index

The LES quality criterion shown here is developed from Ref. [69]. This model is a modification of the derivation used by Pope [70]. The LES quality criterion used here is:

$$I = \frac{k_{res}}{k_{res} + k_{k_{sgs}}} \tag{2.1}$$

with the k_{res} variable defined as the resolved turbulent kinetic energy for the control volume. The k_{sgs} value is the subgrid scale (SGS) kinetic energy which can be expanded to become:

$$k_{sgs} = \frac{1}{C_s} \times \left(\frac{\mu_{sgs}}{\rho \times \Delta} \right)^2 \tag{2.2}$$

In Eq. 2.2, the C_s is the Smagorinsky constant. Delta, Δ, is the cubic root of a cell volume in the mesh. The SGS viscosity is expressed via μ_{sgs}. Finally, k_{res} is the half the magnitude of root mean square (RMS) velocity field components.

$$k_{res} = 0.5 \times \sqrt{(u_{rms})^2 + (v_{rms})^2 + (w_{rms})^2} \tag{2.3}$$

For clarity, it is stated again that this methodology is a criterion commonly used for LES simulation quality assessment.

2.5 Numerical Models and Boundary Conditions

Numerical settings as well as boundary conditions selection for the non-reacting and reacting CFD simulations are described in this section. All simulations were based on the pressure-based solver where the static pressure is obtained from a combination of continuity and momentum equations unlike the the density-based approach where the mass conservation is used to retrieve the density whereas the pressure is calculated from the equation of state. The coupled pressure-velocity scheme is used for all cases in this study ensuring faster convergence over the segregated solver. The pressure based solver use to be reserved for incompressible flow at low speeds while the density based solver handled compressibilty [68]. Both the density based and pressure based solvers have been reformulated to handle a wider class of

problems which is why the pressure based solver can be used in combustion in place of the traditional density based solver. The pressure based solver has been successfully applied in combustion modeling in [69, 71].

Because transient CFD simulations are time-dependent, either for the non-reacting or reacting flows modeled, it requires the calculation of a characteristic flow through time to determine the relevant physical time to extract data during the simulation. For the present modeled fluid volume of the experiment, the convective time selected is 0.0688 s corresponding to the ratio of the overall flame tube length divided by the bulk flow velocity inside the flame tube. Extraction of the simulation data for analysis included 20 time instants equally spaced over this physical flow time. It is important to calculate this physical and characteristic time in order to properly compare CFD simulations to actual experiments.

To start the flow time calculation the length scale is required. The length scale in this case is the diameter of the quartz tube which is 69.85 millimeters. The next step is to acquire a velocity range from either a prior CFD simulation or estimate a velocity range. The velocity range here originated from the RANS case and is 21 to 27 m/s. For the higher time estimate:

$$T1 = \frac{Length\ Scale}{Lower\ Velocity\ Value} \tag{2.4}$$

And for the lower time estimate:

$$T2 = \frac{Length\ Scale}{Higher\ Velocity\ Value} \tag{2.5}$$

These two values from Eq. 2.4 and Eq. 2.5 are then multiplied by five for five flow through times. This gives in the present case a T1 = 0.0165 seconds and T2 = 0.0125 seconds. For safety the simulation was allowed to run to a flow time of 0.0688 seconds to insure that the simulation could be compared to future experiments. Data sampling of the

system was then conducted for 0.06 seconds.

The SBES and FGM modeling strategies used in this numerical study of the laboratory scale burner are now described. The SBES model is a hybrid model combining both RANS and LES turbulence closure models. The boundary layers and the converging nozzle region of the laboratory scale burner are treated with RANS to reduce the computational time. In this framework, the RANS k-omega-shear stress turbulence model is applied in the boundary layer and converging nozzle while in the bulk flow field, the LES is applied with subgrid scale Smagorinsky-Lilly model with Dynamic Stress. Using RANS in the boundary layer saves computational resources and time by avoiding explicit modeling or resolving the smallest scales required by LES to solve especially for the turbulent boundary layers that may form. To do so, the flow solver employs a shield function to switch rapidly between the LES and RANS turbulence closure models. This shield function, f_s, is an explicit term both into the viscous stress tensor expression and into the turbulent eddy viscosity expression [72]. This implementation is shown in the two equations below. Eq. 2.6 is the for the viscous stress tensor:

$$\tau_{ij}^{SBES} = f_s \times \tau_{ij}^{RANS} + (1 - f_s) \times \tau_{ij}^{LES} \tag{2.6}$$

The second equation Eq. 2.7 is the for the turbulent viscosity:

$$\nu_{ij}^{SBES} = f_s \times \nu_{t}^{RANS} + (1 - f_s) \times \nu_{t}^{LES} \tag{2.7}$$

The regions where the RANS k-omega-shear stress transport and the LES subgrid scale Smagorinsky-Lilly model with Dynamic Stress turbulent closure models are applied is given in Fig. 2.4. In the blue region such as the swirler and quartz tube, the LES subgrid scale model is applied whereas in the red region, like the boundary layer and converging nozzle, the RANS closure is applied.

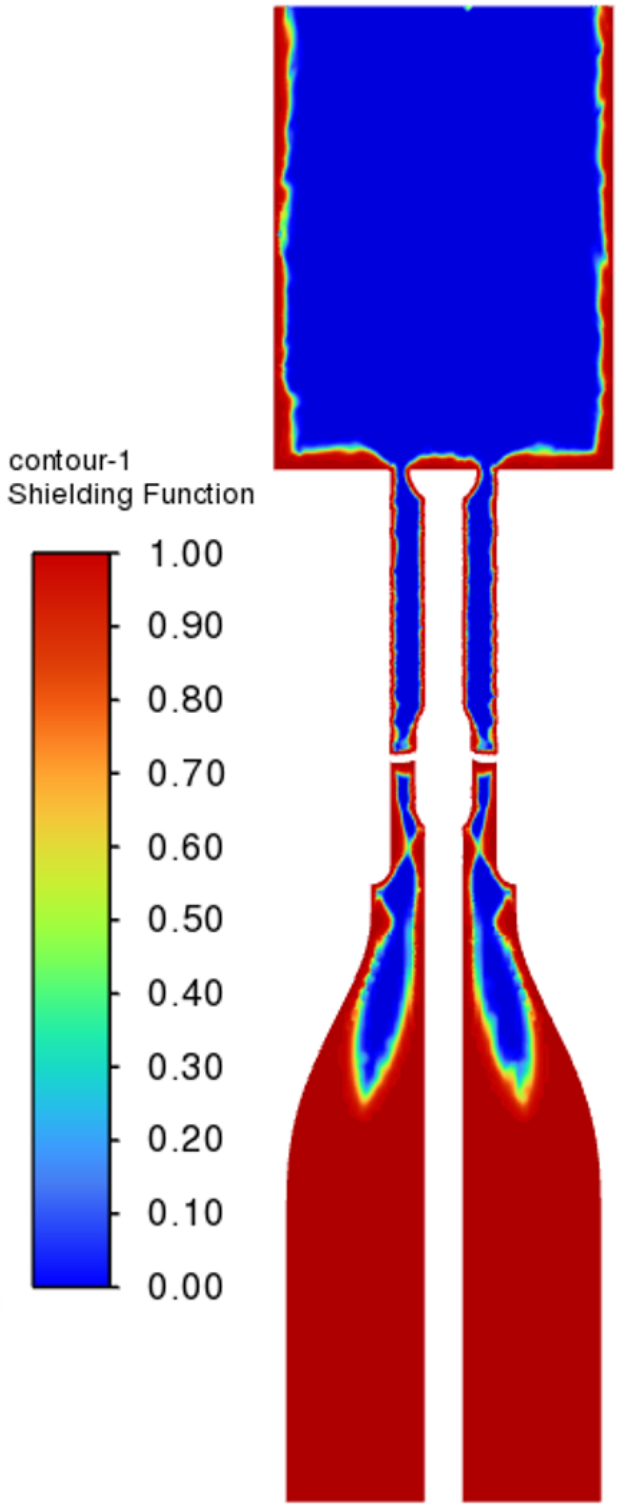

Figure 2.4: View of SBES Map. Red regions use RANS while blue is the LES region.

Turbulence interaction with chemical reactions is complex, and both a spatial and a time-dependant process. To model the combustion, both a combustion model and a chemistry mechanism are required. Combustion is modeled in the present work with the flamelet generated manifold (FGM) model, which represents the thermo-chemistry tabulated with both a mixture fraction and a reaction progress variable via the Bray-Moss-Libby theory [71]. The reaction progress variable, c, and the mixture fraction, z, are normalized in this model [69]. This modeling strategy coupling RANS or SBES and FGM has been validated previously for the prediction of flame temperature and emissions [71, 69]. This modeling approach showed good agreement between experimental data and simulations for the Cabra flame as reported in Ref.[69] as well as for the simulation of a turbulent jet flame [71]. Prediction of flame location is important in determining the entire reacting flow-field especially when dominated by partial mixing or auto-ignition such as in Ref. [69]. To date, the flames that can be modeled with FGM include premixed, diffusion and partially premixed flames.

The flame generated manifold is created from tabulations of 1D steady state flame solutions. The flamelets are solved for in c-space, the reaction progress variable space. The progress variable c is a reduced representation of the overall mixture which allows to tabulates other species present in the chemical reactions. The progress variable c is defined here with [69]:

$$c = \frac{(Y_{H_2O} - Y^u_{H_2O}) + 10 \times (Y_{HO_2} - Y^u_{HO_2})}{(Y^b_{H_2O} - Y^u_{H_2O}) + 10 \times (Y^b_{HO_2} - Y^u_{HO_2})} \tag{2.8}$$

In Eq. 2.8 a progress variable value c of unity corresponds to the burnt products (superscript b) for hydrogen/air flames while a c value of zero corresponds to the unburnt products (superscript u).

The 1D flamelet equations are then solved to build the tabulated chemistry and written in c-space are now discussed and reported here from Ref. [73]. For each species indexed k, one has:

$$\rho\frac{\partial Y_k}{\partial t}+\frac{\partial Y_k}{\partial c}\dot{\omega}_c=\rho\chi_c\frac{\partial^2 Y_k}{\partial c^2}+\dot{\omega}_k \tag{2.9}$$

For the temperature of the gaseous mixture, one has:

$$\rho\frac{\partial T_m}{\partial t}+\frac{\partial T_m}{\partial c}\dot{\omega}_c=\rho\chi_c\frac{\partial^2 T_m}{\partial c^2}-\frac{1}{c_{p,m}}\Sigma_{k=1}^{N}h_k\dot{\omega}_k+\frac{\rho\chi_c}{c_{p,m}}\left(\frac{\partial c_{p,m}}{\partial c}+\Sigma_{k=1}^{N}c_{p,k}\frac{\partial Y_k}{\partial c}\right)\frac{\partial T_m}{\partial c} \tag{2.10}$$

The scalar dissipation term χ_c in c-space is defined with:

$$\chi_c=\frac{\lambda}{\rho c_p}\times|\nabla c|^2 \tag{2.11}$$

Where ω_k is the mass reaction rate of species k, $\mathrm{h}_{t,k}$ is the total enthalpy of species k, and $\mathrm{c}_{p,k}$ is the specific heat at constant pressure of the same species. T_m is the local mixture temperature and $\mathrm{c}_{p,m}$ represents the specific heat at constant pressure of the mixture.

In the combustion FGM model, the transport equation for the mean mixture fraction is Favre density-averaged and can be found in Ref.[68]. The variance for the turbulent mixture fraction is also transported and documented in the same reference. The variance for a given mixture fraction is then used to model turbulence-chemistry behavior. Turbulence-chemistry closure for the source term is modeled within the combustion model with the use of the β-Probability Density Function (PDF). This tabulated data is stored for use during computing. This solves the mean temperature, species mass fraction and density [69]. The number of discrete points for tabulation used is discussed in the reacting flow section. Automated discretization refinement was used in the present article.

The Lewis number, defined as the ratio of characteristic times of heat to mass diffusion is constant and set to unity as muticomponent transport is not taken into account in this initial simulations and preferential diffusion effects are not investigated. The competitive effects between turbulence wrinkling and preferential diffusion are thus not investigated here and will be part of future work. For fully premixed flames such as investigated here significantly above the lean flammability limit in presence of strong turbulence generated by the swirler,

this unity Lewis number is a severe assumption requiring further validation where it could perhaps hold.

Non-Reacting Flow Field Results

Non-reacting simulations were conducted first to establish the flow field and to validate the core experimental burner design. As indicated previously, the non-reacting flowfield examines the core flow features of the burner such as the IRZ, ORZ, and the swirling jets. The first simulation is modeled with RANS and the two equations k-Omega-SST closure. Air and hydrogen are treated as perfect gas. The premixture formed is at equivalence ratio of 0.6. A mass flow inlet and a pressure outlet boundary conditions are selected replicating atmospheric pressure exhaust. The value of the mixture mass flow rate is 3.55 g s^{-1} and the pressure at the outlet is set to one atmosphere. The numerical solver setup follows the boundary conditions. The numerical solver is the couple scheme with a Rhie-Chow distance based flux type. Spatial discretization numerical scheme is second order. A global time step is used and a warped face gradient correction is enabled. The pseudo time explicit relaxation factors were left at the default values. A hybrid initialization method for this study was chosen where an estimate of the mean flow field is formed before the numerical iterative procedure based on provided boundary conditions. Convergence parameters are now described and consisted in residual monitoring and mass conservation verification. The continuity equation, momentum and energy equation's convergence criteria to stop the numerical iterative process were set to $1.0E^{-6}$. Results include contours of velocity components, static pressures, and a mass balance between the inlet and outlet of the burner. The mass balance between the inlet and outlet of the burner was found to be of the order of $1.0E^{-14}$ kg s^{-1} confirming convergence. The simulation's scaled residuals converged in 550 iterations. Figure 2.5 presents the obtained RANS flowfield. The velocity magnitude is provided on the left whereas the tangential velocity is sketched on the right. The strong swirling flow motion is well imparted by the swirler and the inner recirculation zone, the extent of the swirling jets and the tangential velocities well identified as expected by the proposed design.

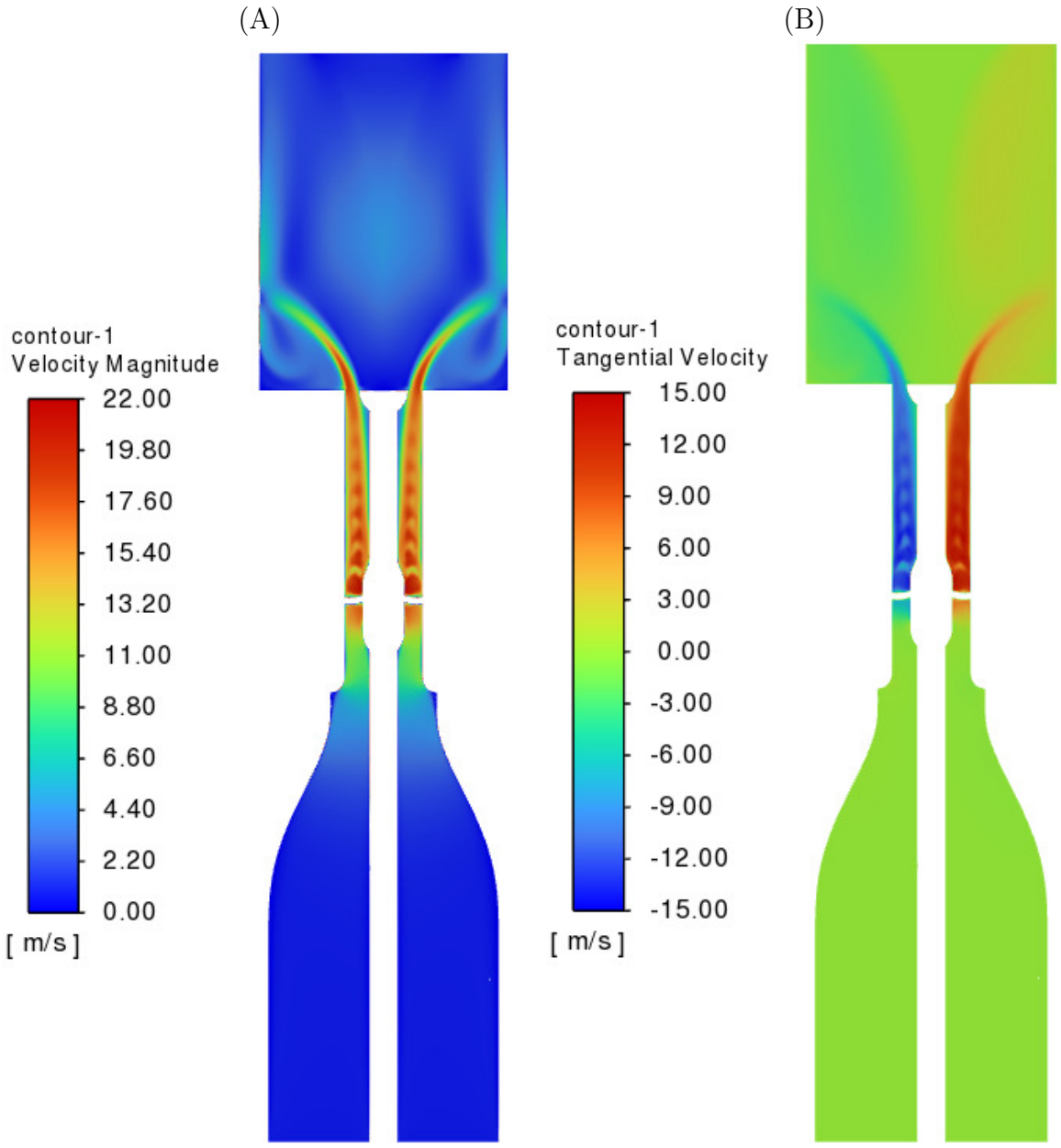

Figure 2.5: (A): RANS velocity magnitude (B): RANS tangential velocity component.

The LES simulation using the Smagorinsky-Lilly subgrid scale model with dynamic stress was conducted next. The timestep size for advancing the solution in time was set to 1.0E^{-6} with the SIMPLEC solver. The LES simulations were primarily done to test the solver setup and to see what the initial flow field looked like. Figure. 2.6 presents the contours of velocity magnitude in Figure. 2.6(A) and tangential velocity in Figure. 2.6(B). The IRZ and ORZ have not formed and the swirling jets are clearly developing. It is observed that the swirler is creating the swirling flow. This simulation will be further continued to enable a direct comparison with the RANS simulation.

Reacting Flowfield and Flame Shape

Once the non-reacting simulations are finished, the reacting simulations then follow. The reacting simulations present the initial results for a premixed hydrogen-air swirl stabilized flame. The setup for the reacting hydrogen air simulations are presented in this section. The base reaction for hydrogen for a given ϕ value can be seen in Eq. 2.12. The mixture fraction z can also be found for the system using the mass fractions of fuel and air or the stoichiometric ratio with the equivalence ratio ϕ.

$$2\,\phi\text{H}_2 + (\text{O}_2 + 3.76\,\text{N}_2) \longrightarrow 2\,\phi\text{H}_2\text{O} + (1\text{-}\phi\text{O}_2) + 3.76\,\text{N}_2 \tag{2.12}$$

For the mixture fraction z is defined using either the mass fractions of the species Z_i, oxidizer $Z_{i,ox}$ and the fuel mass fraction $Z_{i,fuel}$ or using the stoichiometric ratio and the equivalence ratio ϕ:

$$z = \frac{Z_i - Z_{i,ox}}{Z_{i,fuel} - Z_{i,ox}} = \frac{\phi S_a}{1 + \phi S_a} \tag{2.13}$$

where the mass flowrate of fuel is defined with:

$$\dot{m}_f = \phi \times S_a \times \dot{m}_{ox} \tag{2.14}$$

The turbulence closure model used for the reacting simulation is the SBES model except for the ignition sequence conducted with RANS. RANS modeling was used to establish the flowfield before ignition. The SBES is activated for the reacting portion of the simulation.

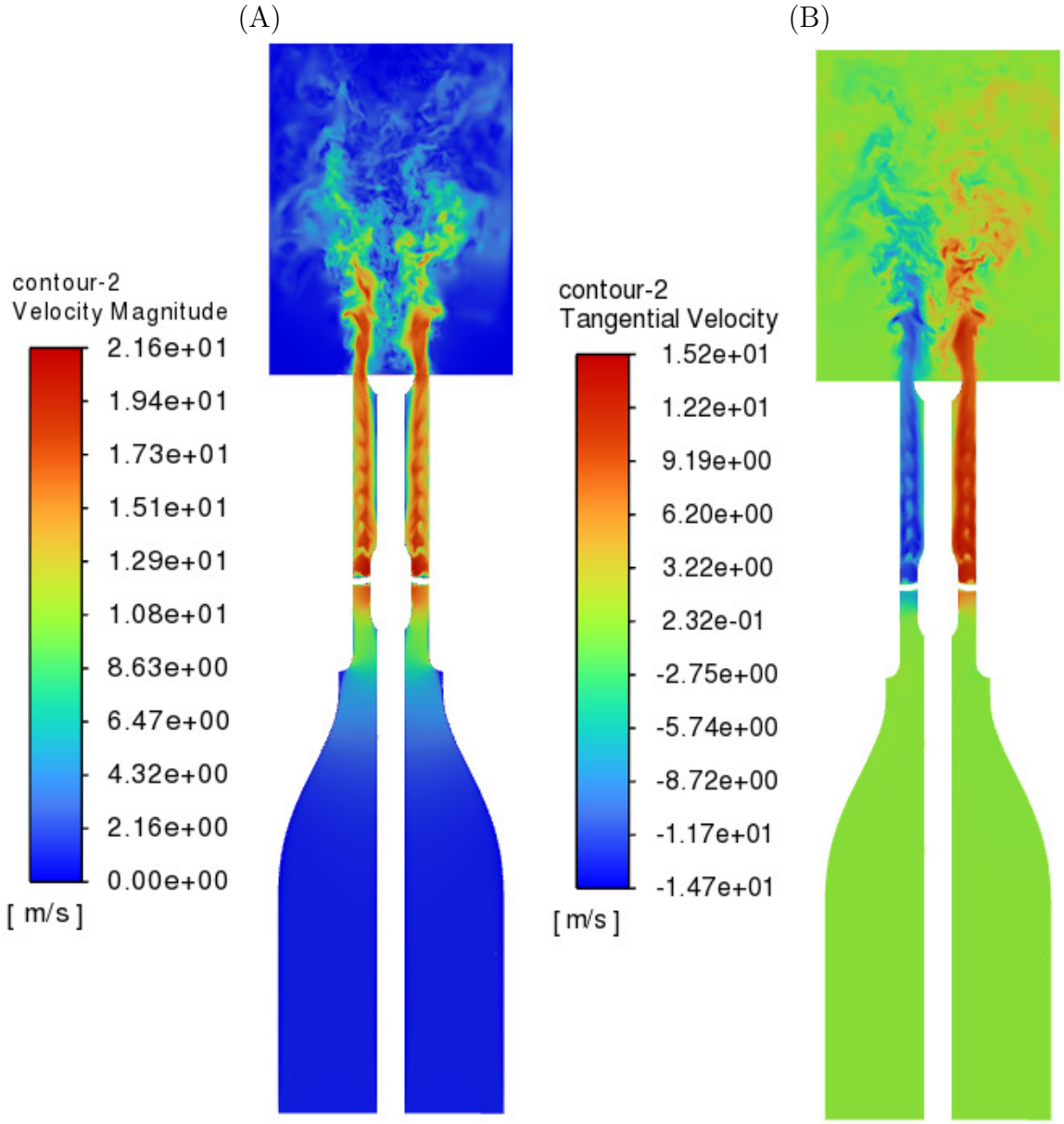

Figure 2.6: Flow speeds taken during the transient before the expected formation of the established flow. (A): LES velocity magnitude. (B): LES tangential velocity component. Velocities are in m s^{-1}.

For combustion, the partially premixed model FGM is chosen [68] described previously. The chemical kinetic model of hydrogen combustion from Ref.[74] is used. The kinetic model contains 9 species and 19 reactions. The number of discretization points for the mixture fraction space is 10 and it is 64 points for the reaction progress space in the FGM model. A lower grid count for the mixture fraction space is used since the hydrogen-air mixture is perfectly premixed at the inlet. At the inlet the molar values of nitrogen, oxygen, and hydrogen are set at a temperature of 300 Kelvin. Automated discretization refinement was used in the present case.The boundary conditions are chosen to be a mass flow inlet at 0.0036 kg $s^{-}1$ with the outlet set to a pressure outlet. The mixture fraction is set to 0.017. For the solution method the selected numerical scheme was the SIMPLE scheme. The flux type chosen was left at Rhie-Chow distance based. Spatial discretization was all second order with momentum set to a bounded central differencing scheme. Gradients are solved using a least squares cell based approach. Under relaxation factors in this case were left at their default values. Reports for probes and iso-surfaces were then set up at various points in the domain to measure variables such as pressure, velocity, or mass fractions of certain species. The residuals were all left at default values. Animations were then setup for static temperature, oh mass fraction, static pressure, and velocity components. The timestep size chosen was $1.2E^{-}05$. The initialization method chosen is standard initialization from the inlet.

Achieving ignition in the reacting simulation is now described. This is done via a patching method. First a patch plane is inserted into the geometry right before the end of the central rod cap. This patching plane will be used to patch the progress variable from 0 to 1 in the solver igniting the mixture and starting the flame. In the numerical solver, the flow is not ignited for 100 iterations (meaning $c = 0$) in RANS to establish a base flow. The flow is then ignited at the patch plane (c is now equal to 1) and the model is ran for 100 more iterations in RANS. It is then switched to the Smagorinsky-Lilly SBES model. Since reversed flow is expected the backflow mixture variance is changed accordingly. The simulation is allowed to run until the flow time and sample time requirements were met. Fig. 2.7 and Fig. 2.8 aid in visualizing the ignition process via the fluid volume CAD and scaled residuals.

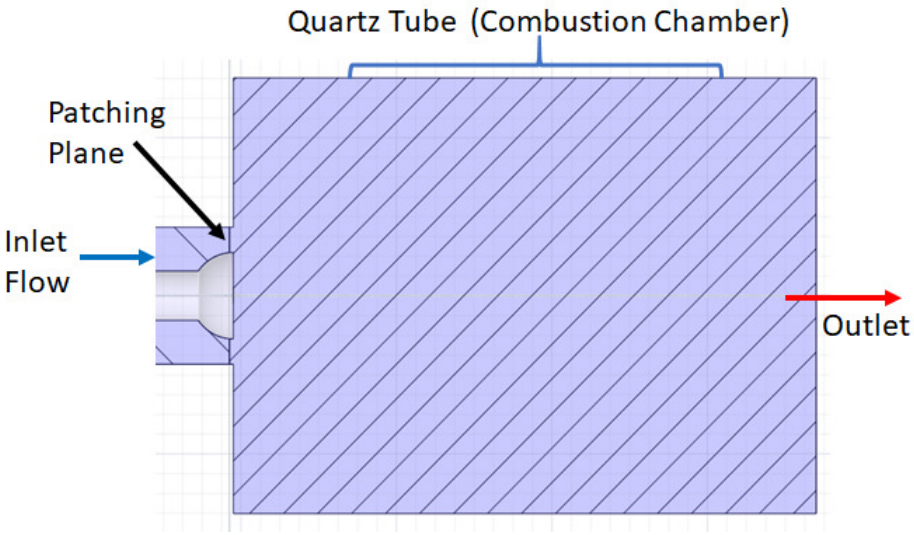

Figure 2.7: Section view of the quartz flame tube showing the patching plane where ignition is applied.

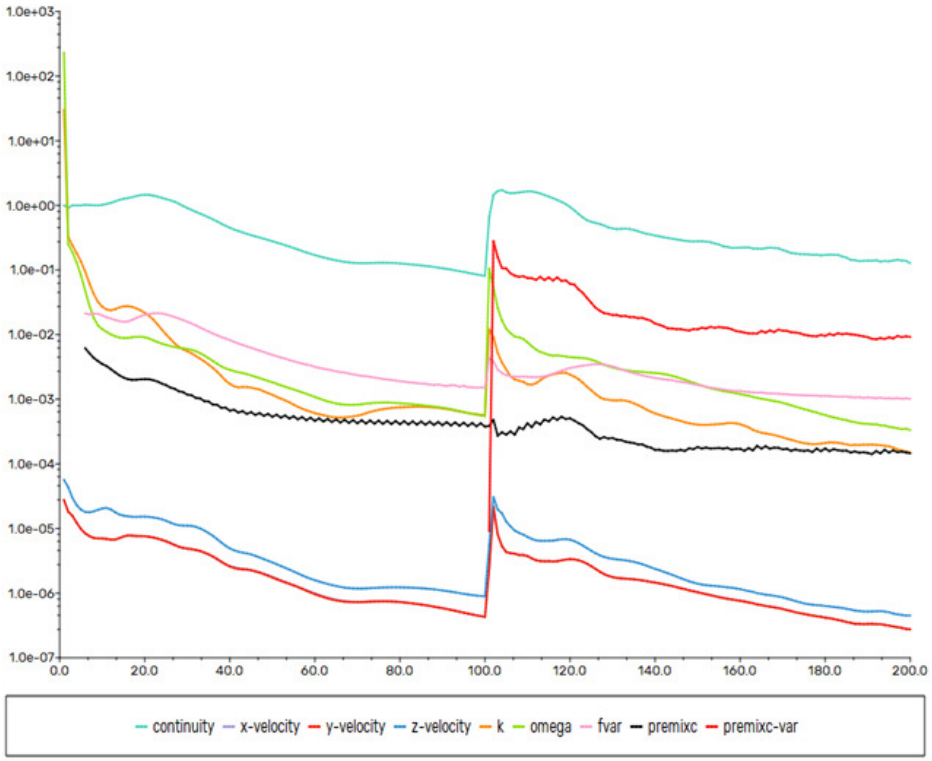

Figure 2.8: Scaled residuals of the ignition process. The sharp rise at 100 iterations is where ignition occurs. The x-axis is the number of iterations. The y-axis is the residual value.

Several results were obtained from the reacting CFD campaign. These include field contours, probe data, animations (not shown here), and a mass balance between the inlet and outlet of the system. The sampling was carried out over 0.06 seconds. The goal here is to assess the flame behaviors and perform exploratory measurements about the system. The reacting simulations took a few days to run on 196 computing cores. Current results show that a swirl stabilized flame is present in the quartz tube Fig. 2.9, Fig. 2.9(d) and no flashback occurs. The flame however does appear to have a small fluctuation in shape. When compared to the length of traditional hydrocarbon fueled flames, this hydrogen flame is much more compact as seen in the mass fraction and static temperature contours. A mass balance calculation between the inlet and outlet was performed to aid in the validation of the simulation. A mass balance of $2.9977E^{-06}$ kg/s is found. This value is near zero which is ideal. Two other calculated values were the laminar flame speed S_l^0 and the turbulent flame speed S_t. S_l^0 was found to be 0.786 m s^{-1} and S_t was found to be 0.813 m s^{-1}. The two values are one of the comparison points between the CFD simulations and the planned experiments. The velocity contours in Fig. 2.10 show the IRZ, ORZ and swirling jets have fully formed as well.

Iso-surfaces and probes mentioned previously were inserted into the domain to take initial measurements. Iso-surfaces in essence allow measurements for variables in a specific region or surface. Probes on the other hand measure at a specific point in the 3D domain. Using iso-surfaces and probe data create an ideal comparison point between the CFD simulations and experiments for many of the variables. Locations to be measured were chosen based off of regions of interest. The two primary regions of interest were the swirler region and the quartz tube. A probe is placed before and after the swirler to check and make sure that the flow is uniform and stable before entering the swirler. Probes are also placed downstream at various points to measure static pressure of the flow. Iso-surfaces are placed at 0.13 meters, 0.14 meters, 0.15 meters and 0.16 meters in the quartz tube to measure various phenomena. A variety measurements from the iso-surfaces and probes are planned on being compared to the experiment such as density, temperature, and mass fractions of various species.

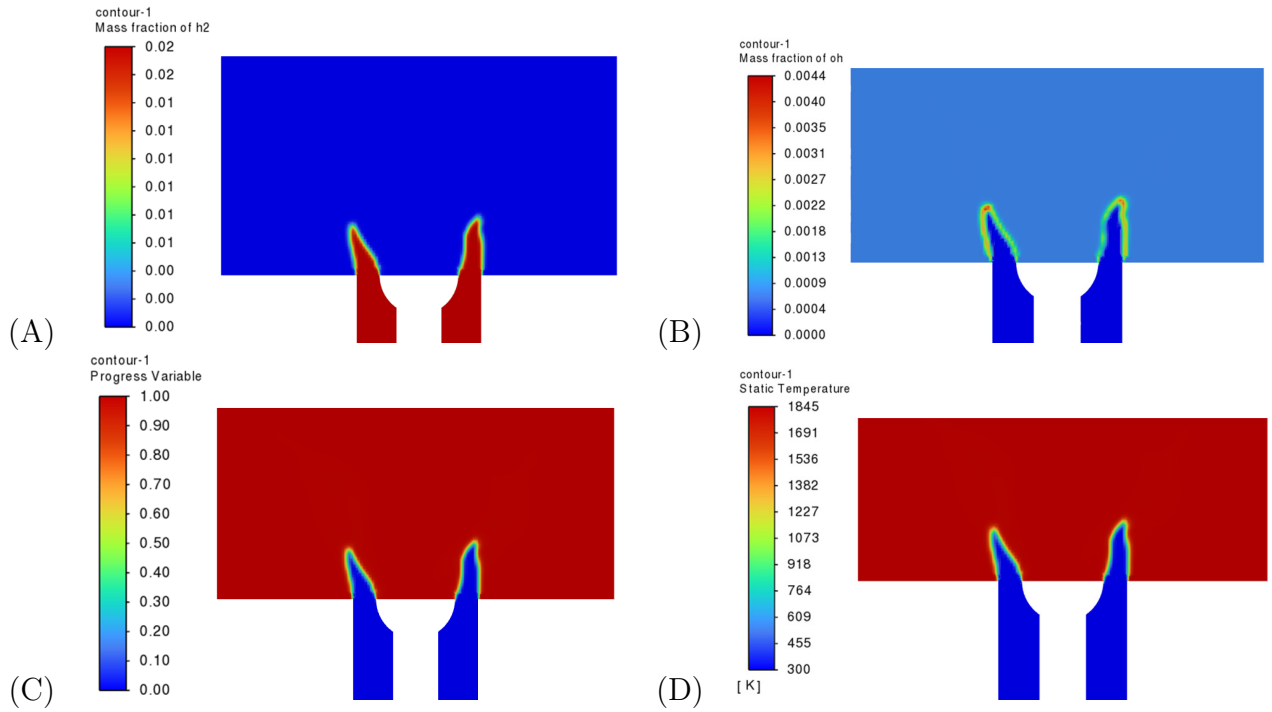

Figure 2.9: (A): Mass fraction of H_2 in the quartz tube. (B): Mass Fraction of OH. (C): Variation of the normalized progress variable C. (D): Static temperature.

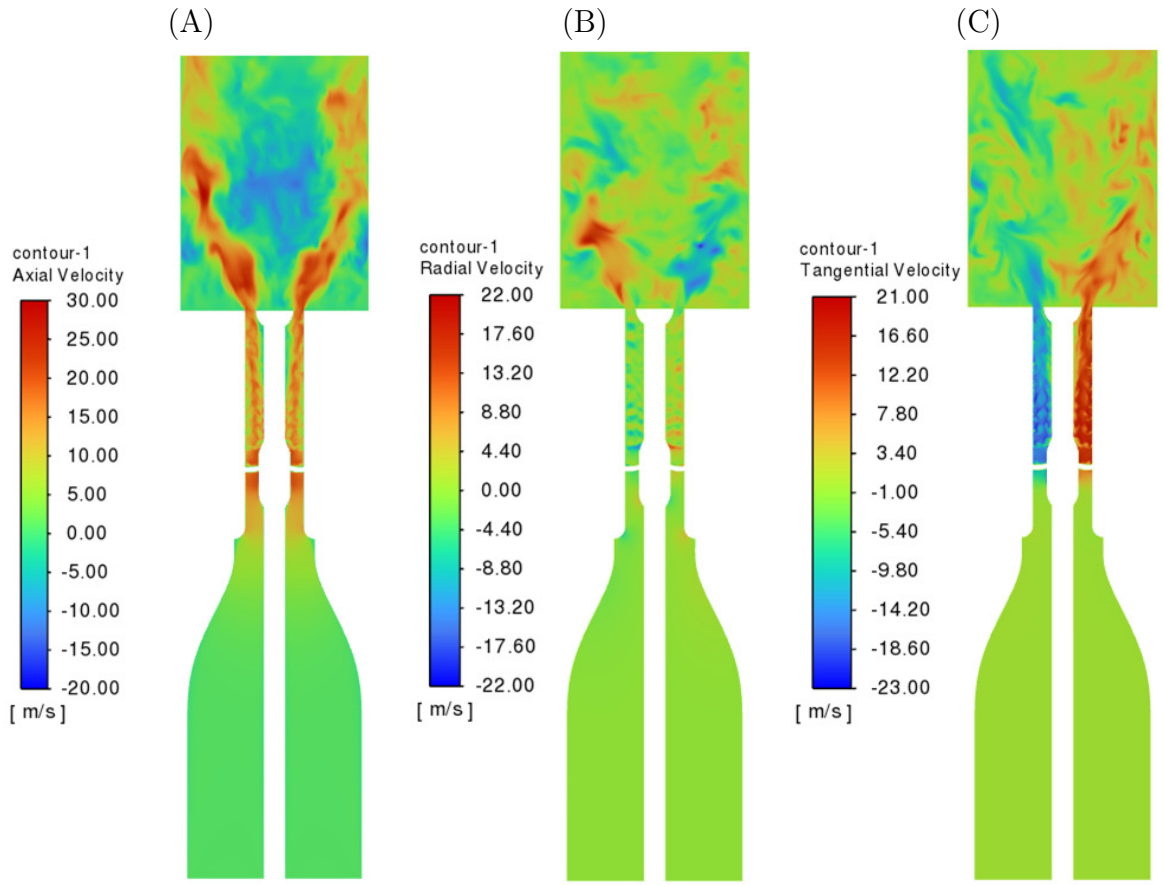

Figure 2.10: (A): Axial velocity component (B): Radial velocity component (C): Tangential velocity component. These are for the reacting case.

2.6 Conclusion

In this work, the initial results of a CFD campaign of a laboratory scale burner are presented. The aim of this work is to aid in the global goal of achieving sustainable, clean aviation via the use of hydrogen-air mixtures. Each aspect of the design study is presented. A description of the burner geometry, fluid volume, mesh, and numerical setup of the non-reacting/reacting simulations is reviewed. A review of the SBES model and FGM model is given along with the ignition method. The main focus of this work is investigating flame stabilization and combustion mechanisms associated with hydrogen-air mixtures for this particular burner design. The results include non-reacting and reacting simulations. This includes several contours including static pressure, velocity components, temperature profiles, various species mass fractions, and variation in progress variable c. Results also include scaled residuals and a mass balance between the system's inlet and outlet to validate the simulation. The mass balance between the inlet and outlet is near zero for both the reacting and non-reacting simulation. The initial swirling hydrogen-air flame shown here is stable. From the simulations the hydrogen flame possess a relatively small height. Flow features such as the IRZ, ORZ, swirling jets, and swirler effects are observed and fully developed in both non-reacting and reacting cases. Future work includes conducting the simulated case shown here with the experimental laboratory scale burner. The next step after the experiment is completed would be to compare the CFD results to the experiment's results. Future CFD work would include a mesh refinement study and implementing new reacting case studies. High resolution DNS simulations are planned in the future which will require immense computational resources to sufficiently model the turbulence, combustion and flame phenomena.

Finally, the design/research methods developed here and utilized along with the initial results in can support the research of unique swirling hydrogen-air flame behaviors in the lean and premixed regime. This will help enable the design, prototyping and testing of a pure hydrogen-air combustion system in a gas turbine engine

Conclusion and Perspective

Conclusion

Advanced turbomachinery development for hydrogen-air mixtures is a key aspect for future propulsion systems aiming to eliminate CO_2 emissions and improve engine performance. A global goal has been set by governments and the aeronautical industry to reduce or eliminate CO_2 and lower the environmental impact from the gas turbine engine. One solution is understanding and researching premixed 100% hydrogen/air flames for a gas turbine combustor. Hydrogen's benefits as a fuel source are well known from an environmental perspective but not a performance one. By making use of a hydrogen-air mixture, the carbon dioxide generated from combustion can be eliminated since no Carbon atoms are present in the fuel. The reduction in the NO_x levels in the final products can be achieved when combusting the hydrogen-air gas in the lean, premixed and swirl stabilized regime. In a prior project, Project Bee demonstrated that hydrogen is a potentially viable fuel in aviation that can greatly improve efficiency and performance of the gas turbine engine. However, there are several engineering challenges for hydrogen propulsion including: hydrogen-air flame stabilization in a highly swirled regime, fuel control system, and cryogenic fuel storage on the aircraft. The specific focus of chapter two is the initial development and design of a laboratory-scale combustor to study lean hydrogen-air flame stabilization in a highly swirled flow. In order to operate the lab-scale combustor in a similar flame regime as the turbofan combustor with hydrogen/air, specific attention is paid to both the engine operating condition and the combustion conditions inside the engine. This is done via the Damköhler and Karlovitz numbers respectively both of which are described. The current design approach presented in this thesis combines a performance analysis of a typical high bypass turbofan

engine, a design review of the laboratory scale combustor, 1D Cantera flame calculation and the companion computational model for 3D CFD simulations. Each aspect from the turbofan performance model to the laboratory combustor device to the non-reacting simulations are described. It is found that the validation code and in house performance model of the turbofan engine have a small percent difference when compared to each other. Cantera 1D flame calculations using a custom mechanism are found to be close to a standard research mechanism (GRI 3.0) and estimate a flame regime where the flamelet generated manifold model applies. The initial non-reacting simulations show the core flow features have formed and all components work as intended.

With the ever rising costs of prototyping and ground testing it is important to understand as much as possible about a device before it is built. This is where CAD and computational fluid dynamics can be of immense aid by simulating an experiment which reduces the overall time and monetary cost of the design process. These analysis methods can potentially find flaws or benefits with a design early on in the design process and provide preliminary results that support real world testing. CFD is applied here to study flame stabilization of hydrogen-air flames. Flame stabilization is a central challenge for future hydrogen powered aircraft and the central focus of this research. Chapter three presents the computational results of a campaign of simulations of a laboratory scale fully premixed hydrogen/air burner.

For the CFD campaign of the laboratory scale burner the overall process discussed step by step from the CAD design to the mesh to the core numerical models and final results. A short discussion of the current literature also presents details on the models and methodology utilized. After the CAD of the burner was finished a fluid volume with a mosaic poly-hexacore mesh is constructed for CFD simulations with a total cell count of 6.2 million. The computational settings and the boundary conditions are described in detail such as the PDF table and SBES turbulence model. The section also reviews results obtained with RANS and LES for the non-reacting flow setup. The method to ignite the mixture for the reacting simulation is presented. A FGM model is used to model combustion and flame behaviors. The results include visualizations of the flowfield with swirling flow velocity components,

species mass fractions, static pressure and temperatures. The results indicate that the current design setup has: (1) a strong inner recirculation zone and an outer recirculation zone, (2) the hydrogen-air flame is compact and stable. The flow structures and the short flame length captured by the simulations for this experimental burner provides a baseline for direct comparison with upcoming experimental measurements.

Perspective

In this work several models are presented and discussed in detail. These models include a parametric performance model of a turbofan engine, Cantera 1D flame code, CAD model of the laboratory scale burner and CFD simulations of the burner. The CFD simulations include a non-reacting and reacting test campaign. The performance model of the turbofan engine has some numerical differences that will be ironed out in order to match the GasTurb data better. The performance model can be applied to other flight regimes such as climb or take-off. Operating maps for engine components such as combustors, compressors or turbines could be constructed as well to give more details about the engine. This would make the code more comprehensive.

The Cantera 1D flame code will be expanded to include more calculations in order gather more information about the 1D flame. The code will be optimized in terms of the computational time without losing calculation quality.

For the burner there are several aspects that will continue to be worked on. Since the core design philosophy of the burner is to be modular in nature new components will be developed. New parts will be developed in a CAD software first then modeled in CFD followed by construction for experiments. These new components include flame arrestors, bluff bodies, and swirlers for example. New CFD simulations that use different numerical models, boundary conditions and burner designs will be conducted to study the combustion behavior under unique conditions. Flame behaviors to be studied in CFD and experiments

include flashback, thermoacoustics, blow off and blowout. Finally, the experimental facilities and equipment required for this type of research is currently being installed within the C-PARC group at UTSI. The methodology and models developed here will serve the goal of building knowledge around premixed hydrogen-air flames in upcoming works. Filling in this knowledge gap will enable a retrofit or construction of a turbofan engine to work with hydrogen-air mixtures in the future.

Bibliography

[1] Jack D Mattingly, Keith M Boyer, and Hans von Ohain. *Elements of propulsion: Gas Turbines and Rockets*. American Institute of Aeronautics and Astronautics Reston, VA, 2006. 1, 4, 5, 30, 32

[2] Nicholas Cumpsty and Andrew Heyes. *Jet Propulsion: A Simple Guide to the Aerodynamics and Thermodynamic Design and Performance of Jet Engines*. Cambridge University Press, 2015. 1, 30

[3] Paul Palies. *Stabilization and Dynamic of Premixed Swirling Flames: Prevaporized, Stratified, Partially, and Fully Premixed Regimes*. Academic Press, 2020. 1, 9, 16, 17, 18, 30, 31, 32, 33, 53

[4] Airbus. A321 neo: The most successful comerical aircraft family ever, 2021. 3

[5] GasTurb GmbH. *GasTurb 14: Design and Off Design Performance of Gas Turbines*. GasTurb GmbH, Aachen, Germany, 2021. 6, 8, 27

[6] Robert D Zucker and Oscar Biblarz. *Fundamentals of gas dynamics*. John Wiley & Sons, 2019. 7, 30

[7] Southwest Research Institute. Numerical propulsion system simulation (npss), 2022. 8

[8] F. Giuliani, A. Lang, T. Leitgeb, J. Woisetschläger, and F. Heitmeir. Using dual laser vibrometry to monitor the stability of gas turbine combustion. In *European Combustion Meeting, ECM2007*, 2007. 9

[9] Caulfield, Christopher, Patil, Sunil, Arguinzon, Carlo, Ansari, Naseem, and Palies, Paul. Initial Numerical Simulations of a Laboratory-Scale Premixed Hydrogen/Air High Swirl Experiment. pages 1–13, Boston, 2023. ASME. 9, 45

[10] Rakesh Ranjan and Noel. Clemens. Insights into flashback to flameholding transition of hydrogen rich stratified swirl flames. In *Combustion Institute Paper 1540-7489, Proceedings of the Combustion Institute 2020*, pages 6289–6297, Austin, USA, 2020. 9, 19

[11] John W. Daily. Laser induced fluorescence spectroscopy in flames. *Progress in Energy and Combustion Science*, 23(2):133 – 199, 1997. 9

[12] John L. Sloop. Liquid hydrogen as a propulsion fuel, 1945-1959, 1978. 10, 11, 12, 13

[13] David Fenn, Willis Braithwaite, and Paul Ordin. Design and performance of flight type liquid hydrogen heat exchanger. In *National Advisory Committee for Aeronautics*, 1955. 11

[14] Rolls Royce. Easyjet and rolls-royce partner on hydrogen technology demonstrator programme, 2022. 14

[15] Pratt and Whitney. Pratt and whitney awarded department of energy project to develop hydrogen propulsion technology, 2022. 14

[16] CFM. Rise program, 2022. 14

[17] Airbus. Zeroe program, 2022. 14

[18] Chris Caulfield, Jonathan Kolwyck, Tate Prater, and Paul Palies. Premixed hydrogen-air swirled-stabilized combustor development. In *AIAA SciTech Forum*, National Harbor, Maryland, 2023. 15, 24, 49, 51

[19] R.K. Cheng, D. Littlejohn, P.A. Strakey, and T. Sidwell. Laboratory investigations of a low-swirl injector with H2 and CH4 at gas turbine conditions. *Proceedings of the Combustion Institute*, 32(2):3001–3009, 2009. 16

[20] P.L. Therkelsen, J. Enrique Portillo, D. Littlejohn, S.M. Martin, and R.K. Cheng. Self-induced unstable behaviors of CH_4 and H_2/CH_4 flames in a model combustor with a low-swirl injector. *Combustion and Flame*, 160:307–321, 2013. 16

[21] D.W. Davis, P.L. Therkelsen, D. Littlejohn, and R.K. Cheng. Effects of hydrogen on the thermo-acoustics coupling mechanisms of low-swirl injector flames in a model gas turbine combustor. *Proceedings of the Combustion Institute*, 34(2):3135 – 3143, 2013. 16

[22] P. Palies, M. Ilak, and R. Cheng. Transient and limit cycle combustion dynamics analysis of turbulent premixed swirling flame. *Journal of Fluid Mechanics*, 830:681–707, 2017. 16

[23] Majid Emadi, Douglas Karkow, Taleb Salameh, Ameet Gohil, and Albert Ratner. Flame structure changes resulting from hydrogen-enrichment and pressurization for low-swirl premixed methane–air flames. *international Journal of Hydrogen Energy*, 37(13):10397–10404, 2012. 16

[24] Majid Emadi, Douglas Karkow, Antonio Melendez, and Albert Ratner. Parameter variations and the effects of hydrogen: An experimental investigation in a lean premixed low swirl combustor. *International Journal of Hydrogen Energy*, 38(13):5401–5409, 2013. 16

[25] T.F. Guiberti, D. Durox, P. Scouflaire, and T. Schuller. Impact of heat loss and hydrogen enrichment on the shape of confined swirling flames. *Proceedings of the Combustion Institute*, 35(2):1385–1392, 2015. 16

[26] Gorkem Oztarlik, Laurent Selle, Thierry Poinsot, and Thierry Schuller. Suppression of instabilities of swirled premixed flames with minimal secondary hydrogen injection. *Combustion and Flame*, 214:266–276, 2020. 16

[27] T. Schuller, S. Marragou, G. Oztarlik, T. Poinsot, and L. Selle. Influence of hydrogen content and injection scheme on the describing function of swirled flames. *Combustion and Flame*, 240:111974, 2022. 16

[28] Davide Laera, Pasquale Walter Agostinelli, Laurent Selle, Quentin Cazères, Gorkem Oztarlik, Thierry Schuller, L Gicquel, and Thierry Poinsot. Stabilization mechanisms of CH_4 premixed swirled flame enriched with a non-premixed hydrogen injection. *Proceedings of the Combustion Institute*, 38(4):6355–6363, 2021. 16

[29] Soufien Taamallah, Santosh J Shanbhogue, and Ahmed F Ghoniem. Turbulent flame stabilization modes in premixed swirl combustion: physical mechanism and karlovitz number-based criterion. *Combustion and Flame*, 166:19–33, 2016. 16

[30] Ianko Chterev and Isaac Boxx. Effect of hydrogen enrichment on the dynamics of a lean technically premixed elevated pressure flame. *Combustion and Flame*, 225:149–159, 2021. 16

[31] Lukas Berger, Konstantin Kleinheinz, Antonio Attili, and Heinz Pitsch. Characteristic patterns of thermodiffusively unstable premixed lean hydrogen flames. *Proceedings of the Combustion Institute*, 37(2):1879–1886, 2019. 17

[32] Jacqueline Chen and Hong Im. Stretch effects on the burning velocity of turbulent premixed hydrogen/air flames. *Proceedings of the Combustion Institute*, 28(1):211–218, 2000. 17

[33] Sheng Yang, Abhishek Saha, Wenkai Liang, Fujia Wu, and Chung K Law. Extreme role of preferential diffusion in turbulent flame propagation. *Combustion and Flame*, 188:498–504, 2018. 17

[34] Wonsik Song, Himanshu Dave, Hong G Im, Swetaprovo Chaudhuri, et al. Local flame displacement speeds of hydrogen-air premixed flames in moderate to intense turbulence. *Combustion and Flame*, 236:111812, 2022. 17

[35] Weijie Zhang, Jinhua Wang, Wenjun Lin, Runze Mao, Hao Xia, Meng Zhang, and Zuohua Huang. Effect of differential diffusion on turbulent lean premixed hydrogen

enriched flames through structure analysis. *International Journal of Hydrogen Energy*, 45(18):10920–10931, 2020. 17

[36] KKJ Ranga Dinesh, H Shalaby, KH Luo, JA Van Oijen, and D Thévenin. High hydrogen content syngas fuel burning in lean premixed spherical flames at elevated pressures: Effects of preferential diffusion. *International Journal of Hydrogen Energy*, 41(40):18231–18249, 2016. 17, 19

[37] Alex. Novoselov, Dominik. Ebi, and Nicolas. Noiray. Accurate prediction of confined turbulent boundary layer flashback through a critically strained flame model. In *ASME Paper GTP-22-1400, ASME Turbo Expo 2022*, pages 1–11, Zurich, Switzerland, 2022. 19

[38] Hao Xia, Wang Han, Xutao Wei, Meng Zhang, Jinhua Wang, Zuohua Huang, and Christian Hasse. Numerical investigation of boundary layer flashback of ch4/h2/air swirl flames under different thermal boundary conditions in a bluff-body swirl burner. *Proceedings of the Combustion Institute*, 2022. 20

[39] Tate Prater, Christopher Caulfield, Gan Xiao, and Paul Palies. Investigation of mixing mechanisms to enable premixed hydrogen combustion. AIAA SciTech Forum, 01 2023. 26

[40] Paul P. Palies. Hydrogen Thermal-Powered Aircraft Combustion and Propulsion System. *Journal of Engineering for Gas Turbines and Power*, 144(10), 09 2022. 101007. 33

[41] Gan Xiao and Paul Palies. Development, comparison, and validation of an all-reactions and all-species h2/o2/n2 mechanism. 2022. 75^{th} American Physical Society Annual Meeting of the Division of Fluid Dynamics. 35

[42] P. Palies, D. Durox, T. Schuller, P. Morenton, and S. Candel. Dynamics of premixed confined swirling flames. *Comptes Rendus Mecanique*, 337(6-7):395–405, 2009. 34, 48

[43] G.H. Markstein. *Nonsteady flame propagation*. Marstein, G.H., Ed., Pergamon Press, 1964. 44

[44] Paul Palies. The flame surface speed budget for turbulent premixed flame stabilization studies. In *AIAA Scitech 2020 Forum*, pages 2–22, 2020. 44

[45] A. C. Benim and K. J. Syed. *Flashback mechanisms in lean premixed gas turbine combustion*. Academic press, 2014. 46

[46] S.L. Plee and A.M. Mellor. Review of flashback reported in prevaporizing/premixing combustors. *Combustion and Flame*, 32:193–203, 1978. 46

[47] A Nauert, Per Petersson, M Linne, and A Dreizler. Experimental analysis of flashback in lean premixed swirling flames: conditions close to flashback. *Experiments in Fluids*, 43(1):89–100, 2007. 46

[48] Dominik Ebi and Noel T Clemens. Experimental investigation of upstream flame propagation during boundary layer flashback of swirl flames. *Combustion and Flame*, 168:39–52, 2016. 46, 47

[49] Dominik Ebi, Rakesh Ranjan, and Noel T Clemens. Coupling between premixed flame propagation and swirl flow during boundary layer flashback. *Experiments in Fluids*, 59(7):1–16, 2018. 46

[50] Vera Hoferichter, Christoph Hirsch, Thomas Sattelmayer, Alireza Kalantari, Elliot Sullivan-Lewis, and Vincent McDonell. Comparison of two methods to predict boundary layer flashback limits of turbulent hydrogen-air jet flames. *Flow, Turbulence and Combustion*, 100(3):849–873, 2018. 46, 47

[51] D Ebi, R Bombach, and P Jansohn. Swirl flame boundary layer flashback at elevated pressure: Modes of propagation and effect of hydrogen addition. *Proceedings of the Combustion Institute*, 38(4):6345–6353, 2021. 46

[52] C. Heeger, R.L. Gordon, M.J. Tummers, T. Sattelmayer, and A. Dreizler. Experimental analysis of flashback in lean premixed swirling flames: upstream flame propagation. *Experiments in fluids*, 49(4):853–863, 2010. 46

[53] Nicholas Syred, Anthony Giles, J Lewis, M Abdulsada, A Valera Medina, Richard Marsh, Philip John Bowen, and Anthony John Griffiths. Effect of inlet and outlet configurations on blow-off and flashback with premixed combustion for methane and a high hydrogen content fuel in a generic swirl burner. *Applied energy*, 116:288–296, 2014. 46

[54] Elliot Sullivan Lewis, Vincent G McDonell, Alireza Kalantari, and Priyank Saxena. Evaluation of a turbulent jet flame flashback correlation applied to annular flow configurations with and without swirl. In *Turbo Expo: Power for Land, Sea, and Air*, volume 84126, pages GT2020–14703. American Society of Mechanical Engineers, 2020. 46

[55] Thoralf G Reichel and Christian Oliver Paschereit. Interaction mechanisms of fuel momentum with flashback limits in lean-premixed combustion of hydrogen. *International Journal of Hydrogen Energy*, 42(7):4518–4529, 2017. 47

[56] Thoralf G Reichel, Steffen Terhaar, and Oliver Paschereit. Increasing flashback resistance in lean premixed swirl-stabilized hydrogen combustion by axial air injection. *Journal of Engineering for Gas Turbines and Power*, 137(7):071503, 2015. 47

[57] Mohammed Al-Fahham, Fares Amer Hatem, Ali Safa Alsaegh, Agustin Valera Medina, Samuel Bigot, and Richard Marsh. Experimental study to enhance resistance for boundary layer flashback in swirl burners using microsurfaces. In *Turbo Expo: Power for Land, Sea, and Air*, volume 50848, pages GT2017–63367. American Society of Mechanical Engineers, 2017. 47

[58] Vera Hoferichter, Christoph Hirsch, and Thomas Sattelmayer. Analytic prediction of unconfined boundary layer flashback limits in premixed hydrogen-air flames. *Combustion Theory and Modelling*, 21(3):382–418, 2017. 47

[59] Stephan Burmberger and Thomas Sattelmayer. Optimization of the aerodynamic flame stabilization for fuel flexible gas turbine premix burners. *Journal of Engineering for Gas Turbines and Power*, 133(10), 2011. 47

[60] Stephan Burmberger, Christoph Hirsch, and Thomas Sattelmayer. Design rules for the velocity field of vortex breakdown swirl burners. In *Turbo Expo: Power for Land, Sea, and Air*, volume 42363, pages 413–421, 2006. 47

[61] Christian Eichler, Georg Baumgartner, and Thomas Sattelmayer. Experimental investigation of turbulent boundary layer flashback limits for premixed hydrogen-air flames confined in ducts. *Journal of Engineering for Gas Turbines and Power*, 134(1), 2012. 47

[62] F Kiesewetter, M Konle, and T Sattelmayer. Analysis of combustion induced vortex breakdown driven flame flashback in a premix burner with cylindrical mixing zone. *Journal of Engineering for Gas Turbines and Power*, 129, 2007. 48

[63] Paul Palies, Ragini Acharya, Andreas Hoffie, and Matthew Thomas. Lean fully premixed injection for commercial jet engines: An initial design study. *ASME Turbo Expo 2019*, GT2019-91653, 2019. 51

[64] Andrea Giusti and Epaminondas Mastorakos. Turbulent combustion modelling and experiments: recent trends and developments. *Flow, Turbulence and Combustion*, 103(4):847–869, 2019. 51

[65] James F Driscoll, Jacqueline H Chen, Aaron W Skiba, Campbell D Carter, Evatt R Hawkes, and Haiou Wang. Premixed flames subjected to extreme turbulence: Some questions and recent answers. *Progress in Energy and Combustion Science*, 76:100802, 2020. 53

[66] Adam M Steinberg, Peter E Hamlington, and Xinyu Zhao. Structure and dynamics of highly turbulent premixed combustion. *Progress in Energy and Combustion Science*, 85:100900, 2021. 53

[67] Carlo Arguinzoni. Five Best Practices for Hydrogen Gas Turbine Combustor Meshing Using Ansys Fluent, May 2022. 53

[68] ANSYS, Inc. *Ansys Fluent Theory Guide*. Ansys Inc., Canonsburg, United States of America, 2022. Release 2022R1. 54, 57, 62, 67

[69] Xia, Yu, Yadav, Rakesh, Verma, Ishan, Nakod, Pravin, Orsino, Stefano, and Li, Shaoping. Numerical Simulations of a Lifted Hydrogen Jet Flame Using Flamelet Generated Manifold Approach. In *Proceedings of ASME Turbo Expo 2022*, volume V002T03A004, pages 1–14, Rotterdam, Netherlands, 2022. ASME. 54, 57, 58, 61, 62

[70] S. B. Pope. Turbulent flows, 2000. 57

[71] Patil, Sunil, Cooper, Judy, Orsino, Stefano, Meadows, Joseph, Valdes, Richard, and Laster, Walter. Investigation of Single-Jet Combustor Near Lean Blowout Conditions Using Flamelet-Generated Manifold Combustion Model and Detailed Chemistry. In *Proceedings of Journal of Engineering for Gas Turbines and Power*, volume 138. Journal of Engineering for Gas Turbines and Power, December 2016. 58, 61

[72] Menter, F.R. Best Practice: Scale-Resolving Simulations in Ansys CFD, 2015. 59

[73] Phuc-Danh Nguyen, Luc Vervisch, Vallinayagam Subramanian, and Pascale Domingo. Multidimensional flamelet-generated manifolds for partially premixed combustion. *Combustion and Flame*, 157(1):43–61, 2010. 61

[74] Li, Juan, Zhao, Zhenwei, Kazakov, Andrei, and Dryer, Federick. An Updated Comprehensice Kinetic Model of Hydrogen Combustion. volume 36, pages 566–575. International Journal of Chemical Kinetics, 2004. 67

Vita

Christopher Caulfield is from the small town of Kingston, Tennessee. After graduating high school he went to Tennessee Technological University where he graduated with a degree in Mechanical Engineering with a Mathematics minor. Chris then went to the University of Tennessee Space Institute to pursue a Master's degree in Aerospace Engineering with the C-PARC Group. Where his thesis focus is combustion and propulsion in gas turbine engines. After graduating from University of Tennessee Space Institute, he chose to pursue a PhD in aerospace engineering at Virginia Tech.